energies

MDPI

Review

A Review of Sensor Applications in Electric Vehicle Thermal Management Systems

Anyu Cheng [1], Yi Xin [1,*], Hang Wu [2,*], Lixin Yang [1] and Banghuai Deng [3,*]

[1] Automotive Electronics Laboratory, School of Automation, Chongqing University of Posts and Telecommunications, Chongqing 400065, China; chengay@cqupt.edu.cn (A.C.); s210331136@stu.cqupt.edu.cn (L.Y.)
[2] Chongqing Qingshan Industrial Co., Ltd., Chongqing 402781, China
[3] Qingling Motors Co., Ltd., Chongqing 400052, China
* Correspondence: s210331124@stu.cqupt.edu.cn (Y.X.); wuhang@tsingshan.com (H.W.); deng70101911@163.com (B.D.); Tel.: +86-(13)-295129592 (Y.X.)

Abstract: With the rapid development of the automotive industry, the application of sensors is of great importance in maintaining the reliability of electric vehicles and ensuring the safe operation of electric vehicles. Faced with the increasing data of thermal management system condition monitoring, sensor detection is widely used in the monitoring of electric vehicle thermal management system. In recent years, a large number of related studies and contributions to the literature have been published. Although a number of reviews have summarized this, these reviews lack an overview of the issues and methods raised in these studies. This paper reviews recent sensor applications for electric vehicle thermal management systems. Currently, battery internal sensors, battery external sensors and related multi-sensor fusion, traditional motor sensors, positionless motor sensors, and component-level sensors of air conditioning systems are the main application sensors in the field of thermal management systems. This article introduces the basic principles of each type of sensor, reviews the relevant applications of various thermal management modules, and summarizes the usage characteristics of each type of sensor. The main problems faced by the existing research on the application of thermal management system-based sensors, such as the detection accuracy of traditional sensors and the detection stability of advanced sensors, are summarized, and the solutions proposed by the existing research are also summarized. Finally, some future research directions, trends, and hotspots are outlined. It is hoped that this review can help readers to understand the problems and existing solutions for thermal-management-system-based sensor applications, and to conduct related research more effectively.

Keywords: electric vehicle; thermal management system; battery system sensor; motor system sensor; air conditioning system sensor; temperature detection

Citation: Cheng, A.; Xin, Y.; Wu, H.; Yang, L.; Deng, B. A Review of Sensor Applications in Electric Vehicle Thermal Management Systems. *Energies* **2023**, *16*, 5139. https://doi.org/10.3390/en16135139

Academic Editors: D.Ganesh Gopal and Sanchari Deb

Received: 3 June 2023
Revised: 17 June 2023
Accepted: 26 June 2023
Published: 3 July 2023

1. Introduction

With the popularity of electric vehicles, their thermal management systems have become a hot topic. The thermal management system of electric vehicles mainly consists of batteries, motors, and air conditioning modules. All three modules require thermal management to ensure the performance and longevity of the vehicle. The battery module is one of the most important components of an electric vehicle, and its temperature has a major impact on the performance and life of the vehicle. By using sensors in the battery module, the temperature and status of the battery module can be monitored in real time, preventing damage and failure caused by high or low temperatures. Commonly used detection sensors include temperature, pressure, current, and voltage, and multi-sensor fusion detection is also a future development direction. The motor module is the power source of the electric vehicle, and its temperature also needs to be monitored and controlled in real time. The sensor can detect the temperature and state of the motor in real time,

help to adjust the working state of the motor, and protect the motor from overheating. Due to the limitations of the traditional sensor detection of the motor module, in recent years, the position sensorless technology has used the characteristics of the motor itself and the control algorithm to realize the temperature control and position estimation of the motor. The air conditioning system is also a very important part in electric vehicles. The air conditioning system can not only affect the air quality inside the car but also improve the driving comfort by adjusting the temperature inside the car. The application of sensors in the air conditioning system can monitor parameters such as temperature and humidity in the car and help to realize automatic temperature control.

Overall, the use of sensors in the thermal management system of electric vehicles is crucial. By monitoring the temperature and status of various parts in real time, the thermal management system can more accurately control the temperature of the vehicle and improve the performance and lifetime of the vehicle. In the future, with the continuous advancement of technology, the application of sensors will continue to expand and usher in innovation, providing more complete technical support for the thermal management system of electric vehicles.

2. Research Progress on Sensors for Battery Thermal Management System

Many reviews published in recent years have summarized the commonly used sensors in electric vehicle battery modules, namely: current sensors, voltage sensors, temperature and humidity sensors, pressure sensors, and position sensors. However, there are some differences, such as grouping temperature and pressure or current and voltage into a single category [1]. In addition, some new sensors [2] have also been gradually applied to battery modules, namely: fiber Bragg grating sensors, flexible film sensors, semiconductor gas sensors, digital image sensors, laser displacement sensors, and multi-beam pressure sensors [3]. They are applied to various parts of the battery to detect various indicators and prevent losses caused by battery thermal runaway. Therefore, this paper summarizes the main detection sensors based on battery modules into the following categories: internal detection of battery modules, external detection of battery modules, and multi-sensor fusion detection of battery modules. This section introduces the application status of some commonly used battery detection sensors in the field of battery thermal management. In order to better sort the existing literature, the introduction of the research status is mainly carried out from the perspective of the main problems addressed by the literature and the improvement methods.

2.1. Sensors Inside the Battery Module

Changes in the internal temperature of the battery have a great impact on the battery, so the internal temperature of the battery is also a very important monitoring parameter. When the battery is in a high temperature state, organic materials such as the separator and electrolyte in the battery are unstable, and oxygen will be released near the positive electrode of the battery, which satisfies the three elements of combustion, so the result of thermal runaway is generally accompanied by rapid combustion. In order to prevent serious safety problems of lithium-ion batteries caused by thermal runaway, researchers have extensively investigated protective measures such as PTC, safety valves, and thermal conductive films. At the same time, they have conducted research on battery design, battery manufacturing processes, and battery management systems. Therefore, it is necessary to use the internal sensor of the battery to monitor [4] the change in the internal temperature of the battery in real-time to avoid irreversible damage to the battery due to thermal runaway.

2.1.1. Fiber Bragg Grating Sensor

Yang et al. [5] were the first to study the FBG (Fiber Bragg Grating) sensor on lithium-ion battery technology. Using three coin cells, the temperature of two sections was measured with FBG. In addition, the temperature on the plane and on the sides of the cylindrical cells was also measured. The calibration of the FBG sensor showed a linear response in the

range of 0 to 60 °C. Calibration measurements showed a sensitivity of 10 pm/°C. It can be concluded that the FBG temperature sensor has sufficient thermal response compared to the thermocouple. Despite the success of temperature sensing on Li-ion batteries using FBG sensors, quantification remains difficult. Sommer et al. [6,7], in collaboration with LG Power Company, developed a new embedded FO (Fiber Optic) sensor to monitor the internal temperature and voltage changes in Li-ion batteries. Fiber optic sensors are embedded on the electrodes in the pocket battery. Experiments show that its seal integrity, capacity retention, and projected cycle life are comparable to advanced xEV batteries without embedded sensors. This work focuses on the estimation of state of charge (SOC) and state of health (SOH) using measurements from embedded sensors. The results show that the strain measured with the FO sensor can be used to estimate SOC with an error of less than 2.5% under different temperature conditions and dynamic cycling conditions. This work establishes the possibility of embedding FO sensors in large format cells as a low-cost, field deployable option for directly monitoring the internal cell status of the BMS (Battery Management System) in xEV and other advanced batteries. Fortier et al. [8] integrated an FBG sensor into a Li-ion coin cell, used the FBG sensor to record strain and internal and external temperature, and evaluated the battery performance at a cycled C/20 rate. The FBG sensor was placed between the inner electrode of the coin cell and the separator layer toward the most electrochemically active area using optical-based NOA65 as a sealant. The results show that the inside of the battery has a stable strain behavior during the charge–discharge cycle and that there is a temperature difference of about 10 °C between the inside of the battery and the surrounding environment. When overcharged, the sensitivity of the fiber optic strain sensor can reach 50 times that of the temperature sensor. Therefore, monitoring surface strain can improve system safety and effectively prevent thermal runaway of the battery body. Novais et al. [9] studied the FBG temperature measurement of Li-ion pocket battery. Two optical fibers inscribed with two Bragg gratings were used for internal and external temperature measurement. The chemical resistance of the silica optical fiber was tested in an electrolyte containing LiPF6 salt. After two weeks of storage in the electrolyte, only a very small amount of Si was found to dissolve, indicating that this type of fiber is not sensitive to the electrolyte. The average sensitivities of the external and internal FBG sensors are 8.40 and 10.255 pm/°C, respectively, in a temperature range of 10–35 °C. It was concluded that the optical FBG temperature sensor can detect temperature changes at multiple locations inside and outside with excellent response speed. However, these FBG sensor measurements were not validated against temperature measurements from other sensors. Meyer et al. [10] implanted FBG sensors in battery packs to monitor their temperature changes. Each cell of the battery pack was monitored at predetermined hot spots using FBG temperature sensors. Thermistors were used as standard temperature sensors and attached to the terminals of every fourth battery. A clear difference was found between the thermistor and the FBG sensor. During fast charge, the maximum temperature difference between the hottest and coldest batteries is 15 °C. The relative accuracy of the FBG sensor was determined to be ±0.05 °C, while that of the thermistor was only ±1 °C. It follows that integrating FBG sensors on each battery can provide more accurate measurement information to the BMS. In the battery module, the FBG sensor is connected to the BMS through a wiring harness, and excessive wiring harnesses will reduce the sensitivity of the sensor. To solve this problem, Xu et al. [11] developed a temperature measurement system based on fiber grating technology that can be directly installed on the positive and negative poles of lithium batteries, with a temperature range of 5.0–85.0 °C and a measurement accuracy of 0.01 °C, which can accurately detect the temperature of each battery in the module with only one optical fiber. It can save module space, reduce mutual interference, and realize the accurate management of real-time battery status. Wang et al. [12] monitored the temperature field and bulging deformation of 18650 lithium battery packs by constructing 4 channels and 16 double-clad FBG points. The system primarily consists of a demodulator, FBG sensors, and a monitoring host computer. The demodulator decodes the wavelength signals from the

FBG array, which are then transmitted to the monitoring host computer via a data link. By correlating the decoded information with standardized data, the corresponding real-time environmental temperature conditions can be obtained. As shown in Figure 1a,b.

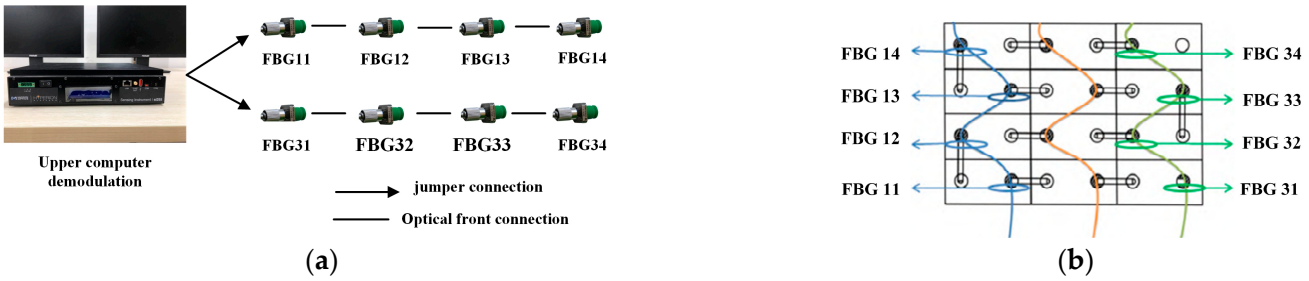

Figure 1. (**a**) Schematic diagram of lithium battery pack temperature monitoring system; (**b**) layout diagram of 18650 lithium battery pack double clad FBG.

As shown in Figure 2a,b, the abnormal temperature rise point has a corresponding temperature sensitivity of 10 pm/°C and a resolution of 0.1 °C, and the double-clad FBG attached to the surface of the lithium battery case can also monitor the bulging deformation on the surface of the battery case. The longitudinal pressure and strain sensitivity is up to 142 pm/N.

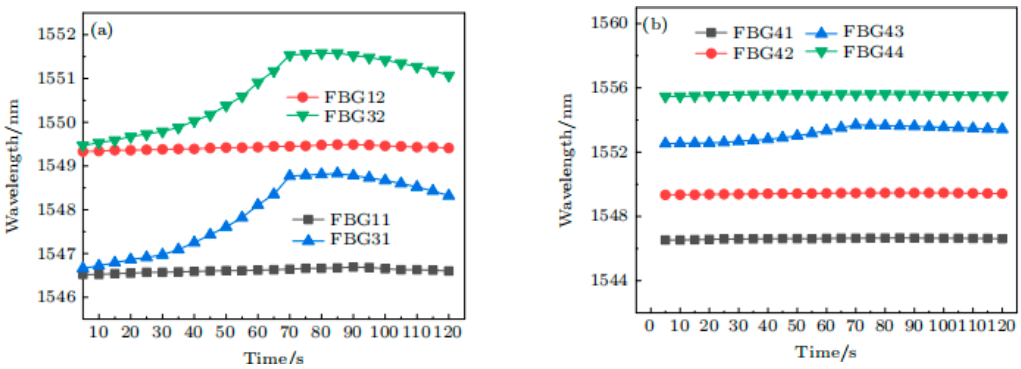

Figure 2. (**a**) Comparison of temperature monitoring of channels 1 and 3 of the temperature field monitoring system; (**b**) channel 4 battery bulge monitoring comparison [12].

Amietszajew et al. [13] used polyamide coating to seal the bare optical fiber in a stable temperature range (−270~300 °C) and passed through the aluminum tube to form a strain protection layer. A layer of fluorinated ethylene propylene heat-shrinkable skin was added on the surface of the aluminum tube to slow down the erosion of the electrolyte. Components prepared in this way can withstand the electrical, chemical, and mechanical stresses experienced during cycling. The fabricated sensor assembly was inserted into the center of a commercial 18650 battery to measure the internal temperature. In addition, a high-precision thermocouple was used to measure the temperature of the outer surface of the battery and the ambient temperature. In addition to the temperature sensor, a lithium metal reference electrode was used. By using the FBG sensor, thermocouple and reference electrode, the thermal and electrochemical response of the battery can be obtained. Based on measurements, the electrochemical and thermal safety limits are not exceeded when the battery is charged at a rate that is 6.7 times higher than the base rate. Therefore, this study shows that there is great promise for performance optimization by integrating an internal temperature sensor and applying a reference electrode.

Huang et al. [14] demonstrated the simultaneous decoding of temperature and pressure of electrochemical cells using FBG sensors carried by conventional single-mode or microstructured optical fibers, applying it to commercial 18650 cells with high accuracy. By tuning the fiber morphology, decoupling temperature- and pressure-dependent wavelength

changes with high precision, developing an economical binary interrogator, and identifying an appropriate transfer function, the FBG sensor is more adaptable to the target system environment and can be used to track such things as interphase between solid electrolytes. Chemical events such as formation and structural evolution. These findings provide a scalable solution for screening electrolyte additives, rapidly identifying optimal formation processes for commercial batteries, and designing battery thermal management systems with improved safety.

2.1.2. Flexible Thin Film Sensors

In addition to using FBG sensors to measure the internal temperature of the battery, Lee et al. [15] first proposed a miniature flexible thin-film RTD (Resistance Temperature Detector) to monitor the internal temperature of Li-ion batteries in situ. The authors show that the sensor responds quickly, can accurately measure the battery temperature, and is easily mass producible. Flexible thin-film micro-RTDs are based on depositing a 200 nm metal layer on a substrate and monitoring its resistance as a function of temperature. The sensor resistance showed a linear behavior for three consecutive cycles in the temperature range of −20 to 90 °C. However, linearity was not quantified; neither stability over three cycles nor calendar stability was shown, which is very important if these sensors are used inside batteries. The author integrated two miniature thin-film RTDs inside the pouch battery and used thermocouples on the surface of the battery. By comparing the temperature changes inside and outside the battery, it was found that the thin-film RTD sensor responded faster, and the internal temperature of the battery was higher than the surface temperature. Zhu et al. [16] developed a new intercalation method by removing a small portion of the active material on the positive electrode of battery to integrate thin-film RTD sensors. This method can attenuate the influence of the sensor on the capacity loss and damage of the active material. The results of long-term cycling experiments show that, compared with ordinary batteries, the corrosive environment of the battery has no effect on the thin-film sensor, and the battery inserted into the thin-film sensor can maintain good cycling performance. So far, internal temperature measurements for commercial Li-ion batteries have been successfully performed. The thickness of the hot junction of the thin-film thermocouple sensor is mostly on the order of microns, which can accurately measure changes in transient temperature. The experimental method is shown in Figure 3.

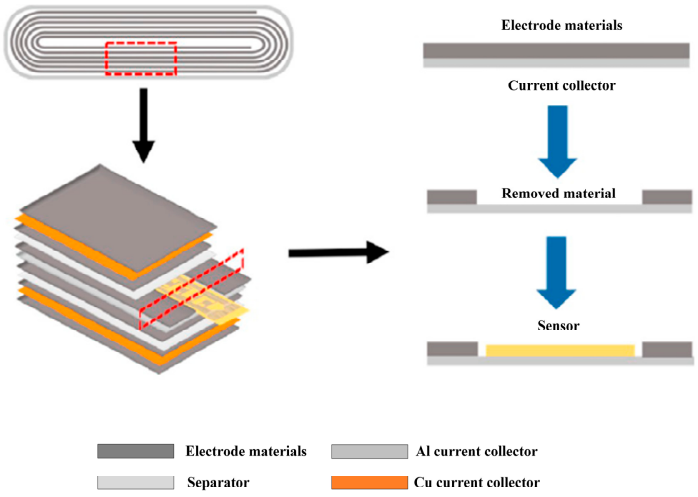

Figure 3. Insert the thin film sensor into the bag battery, remove a small piece of active material, and connect the sensor to this small area at the same time [16].

Mutyala et al. [17] and Pan et al. [18] integrated a flexible TFTC (thin-film thermocouple) into the battery for internal in situ temperature monitoring. K-type thermocouples were sputtered onto a glass substrate and then transferred to a thin copper foil. After insulation with polyimide, the thermocouple is integrated into the pouch cell. The junc-

tion size of the TFTC is much smaller than that of a thin-film RTD, which can provide higher spatial resolution. Unlike thin-film RTDs, TFTCs are insensitive to strain-induced resistance changes. Measurements using integrated flexible thin-film thermocouples are promising, but for the continuous monitoring of battery health, the long-term effect of the sensor material on battery performance needs to be investigated. To measure the internal battery temperature, Martiny et al. [19] developed a matrix of thin-film thermocouples. Nickel and copper were used as different materials for the thermocouple substrate and sprayed onto the Kapton membrane. A layer of parylene was added for protection. The fabricated sensor was less than 27 μm thick and was integrated into a lab-scale pouch battery. At a cycling rate of C/9 [20], the sensor had little effect on battery performance, but the protective coating was damaged during battery assembly and subsequently became unstable due to corrosion. The first thermocouple matrix was improved by using a Kapton foil coating instead of a Parylene coating. Although Kapton increases the sensor thickness to 54 μm, it improves thermal stability and creates a more uniform sensor because the substrate is also Kapton. However, the improved sensors have also encountered stability problems, and it is necessary to improve the fabrication process to ensure long-term sensor stability. The next step is to improve the stability by using liquid polyimide. In 2021, Zhu et al. [21]—at the Beijing Institute of Technology—attached a thin-film strain gauge sensor to the active material of the positive electrode plate of a cylindrical 18650 lithium-ion battery, installed it in the center of the aluminum collector, and measured the strain inside the battery in situ. Studies have shown that the strain change regarding 18650 Li-ion batteries during the charging–discharging process can be divided into three stages. These three stages are mainly caused by the transformation of the graphite negative electrode interlayer spacing during the lithiation/silicidation process. The circumferential strain of 18650 lithium batteries with different silicon contents in the negative electrode has been further investigated [22]. The measured strain curves adequately reflect the volume expansion characteristics of the negative electrode. During battery operation, the volume expansion of the negative electrode determines the circumferential strain. During charging, the strain increases, while during discharging, the strain changes in the opposite direction.

2.1.3. Semiconductor Gas Sensor

Jin et al. [23] conducted an overcharge experiment on a lithium iron phosphate battery pack and used gas sensors to monitor six gases (H_2, CO, CO_2, HF, HCL, and SO_2) generated by the battery during thermal runaway. In the experiment, the characteristic gases were all detected by the corresponding gas sensors, and hydrogen was identified earlier than other gases. At t2 = 990 s, the hydrogen sensor detected the release of H_2 gas, and at t3 = 1425 s and t4 = 1570 s, the battery smoked and caught fire, respectively, providing valuable time for remedial action. Experiments have confirmed that, in the early stages of battery pack overcharge, lithium dendrites are precipitated from the negative electrode, react with the negative electrode binder, and produce H_2, which occurs earlier than the side reactions that produce other characteristic gases. Therefore, monitoring hydrogen helps to detect safety accidents in the overcharging process earlier. Guo Dongliang et al. [24] investigated the safety warning performance of gas sensors for lithium iron phosphate batteries. A hydrogen sensor was installed at a distance of 0.4, 1.0, and 1.8 m above the Li-ion battery, and an oxygen sensor was installed at a distance of 1.8 m. The sensor faces the pressure relief valve port in the battery. Studies have shown that the volume fraction of oxygen during the thermal runaway process of the battery remains basically unchanged at about 20.6%, and no oxygen is produced during the experimental period. At t = 2544 s, the hydrogen sensor at the bottom detected a sharp increase in hydrogen content, 88 s earlier than the opening of the pressure relief valve. At t = 2618 s, the lower hydrogen sensor detects that the hydrogen concentration has reached the set alarm value of 50 mg/L and activates the alarm. Comparing the hydrogen sensors installed at three different heights, the middle and top sensors lagged behind the bottom sensors by 23 and 30 s, respectively. The above three sensors are built into the battery system, which can sensitively detect the

temperature, voltage change, and gas change inside the battery to provide early warning of potential safety hazards.

Sensors based on internal battery detection can be classified into three main types. We conducted an analysis on their detection methods, advantages, and disadvantages, and the following table lists the relevant research papers related to these sensors. As shown in Table 1.

Table 1. The literature on sensors based on internal battery detection.

Sensor	Advantages	Disadvantages	Documents
Fiber Bragg Grating Sensor	1. It can be small in size, anti-electromagnetic interference, non-conductive, and chemically inert. 2. It can be multiplexed, attached to the surface of the battery, and embedded in the battery. 3. Applicable to commercial battery stress and strain, temperature monitoring, and detection	1. Sensitive to multiple physical parameters; there is a large cross-sensitivity, such as strain and temperature. 2. There are certain differences in the calibration of FBG sensors.	[5–14]
Flexible Thin Film Sensor	1. Small in size, high sensitivity, and good dynamic response ability. 2. It is easy to integrate, has good mechanical properties and other characteristics, and is widely used in industrial production.	1. When measuring the internal stress of the battery, it will be disturbed by the electrolyte, which is prone to failure. 2. The inherent electromagnetic shielding problem of the battery.	[15–22]
Semiconductor gas sensor	1. Fast response time and low detection concentration. 2. Has an early warning effect.	1. Low detection accuracy and complex gas cross-interference.	[23,24]

2.2. Sensors Applied on the Outside of the Battery Module

With the rapid development of electric vehicles, the demand for lithium-ion batteries is increasing. The changes in pressure, temperature, and state of the lithium dendrites inside the battery will have a greater impact on the life, capacity, efficiency, and safety performance of the battery. Specifically, the pressure and temperature changes will reduce the safety performance, life, and efficiency of the battery [25]. The most direct and simple way to apply a sensor to a battery is to install the sensor on the outside of the battery, which can directly detect various damages on the outside of the battery. At present, research in this field has achieved considerable results.

2.2.1. Digital Image Correlation Sensor

Zhu et al. [26] developed an in situ temperature measurement technique for Li-ion battery packs that has little impact on the electrochemical performance of Li-ion batteries. In the specific design, one end of the lithium battery is sealed with optical glass, which allows an infrared camera to monitor the pack temperature in real-time through the optical glass during charging and discharging. The measuring device is shown in Figure 4.

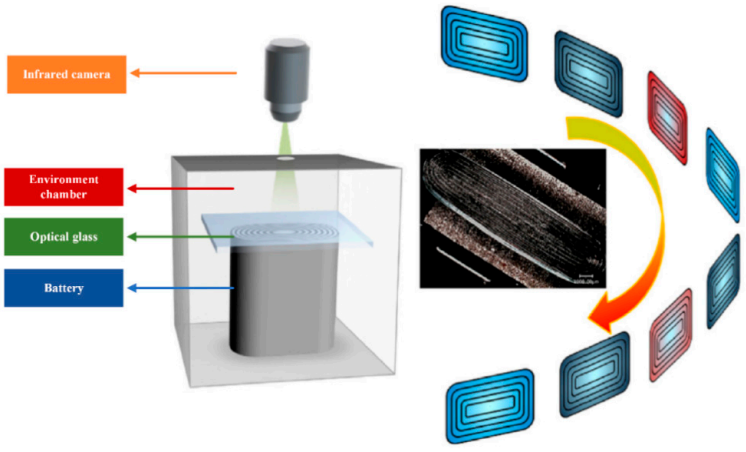

Figure 4. In situ measurement device for lithium-ion battery pack temperature [26].

As shown in Figure 5(1)–(4) the observations show that the temperature is different during charging and discharging. At the end of the 2 C rate discharge process, the maximum temperature difference between the inside and the surface of the visualized Li-ion battery is 2.0 °C. This suggests that it is more important to analyze the effect of temperature on the thermal safety of high capacity Li-ion batteries.

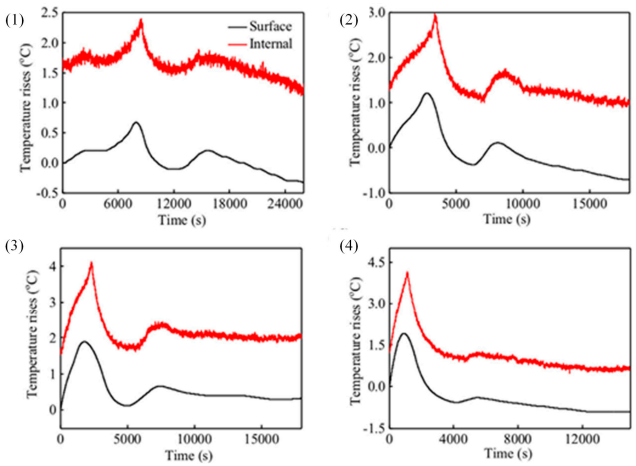

Figure 5. Comparison of internal and surface temperature rise evolution during the discharging and charging processes. (**1**) 0.5 C, (**2**) 1 C, (**3**) 1.5 C, (**4**) 2 C [26].

Chen et al. [27] used micro-scratch and two-dimensional digital image correlation DIC (Digital image correlation) coupling technology to study the role of binders in the mechanical integrity of lithium-ion battery electrodes and established a composite material by creating a micro-scratch model and decoupling the composite material model. This method can provide new guidance for binder selection and electrode design and help to lay the foundations for modeling the mechanical and thermal properties of lithium-ion battery porous electrodes. Qi et al. [28] also used 2D digital image correlation analysis to provide the corresponding deformation and strain fields, showing expansion and contraction. By combining experimental measurements and theoretical analysis, the unexpected shrinkage during lithiation is explained by the stiffness of graphite during lithiation. The results confirm that the increase in graphite crystallite volume during lithiation is mainly accommodated by a decrease in composite (or particle) porosity. Changes in porosity can seriously affect battery power. Jones et al. [29] used digital image correlation to measure the strain induced in Li-ion battery electrodes during lithiation and delithiation. Composite graphite electrodes are cycled at a constant current in a custom battery cell, while optical images of the electrode surface are captured in situ. Chen et al. [30] went on to examine the relationship between discharge capacity and mechanical deformation state using in situ imaging of the working electrode surface inside a custom-made CR2032 lithium coin cell. Digital image correlation was used to quantify electrode strain throughout the discharge–charge process, and the study demonstrated a decrease in discharge capacity with repeated cycling. An increase in residual electrode strain was also observed. In traditional DIC (Digital Image Correlation) techniques, strain data are limited to two dimensions (x and y directions). The working principle involves the use of artificial white light illumination or natural light to observe the random grayscale intensity distribution on the surface of an object in order to capture deformation information. A camera digitally records the surface images of the object before and after deformation. These images are then matched and digitally processed to obtain information about the expected deformation. As is shown Figure 6.

To allow three-dimensional measurements (x, y, and z directions), multiple synchronized stereo sensors are required, combined with photogrammetry theory. Three-dimensional measurements provide a more complete description of cell volume changes during typical electrochemical operations. Leung et al. [31] first proposed the application of 3D digital image correlation for the real-time displacement and strain analysis of pouched

Li-ion batteries. During the electrochemical charge–discharge process, due to the expansion and contraction of the internal structure, the displacements in the x, y, and z directions change under different charge states, and the internal state of the battery is judged by analyzing the change value.

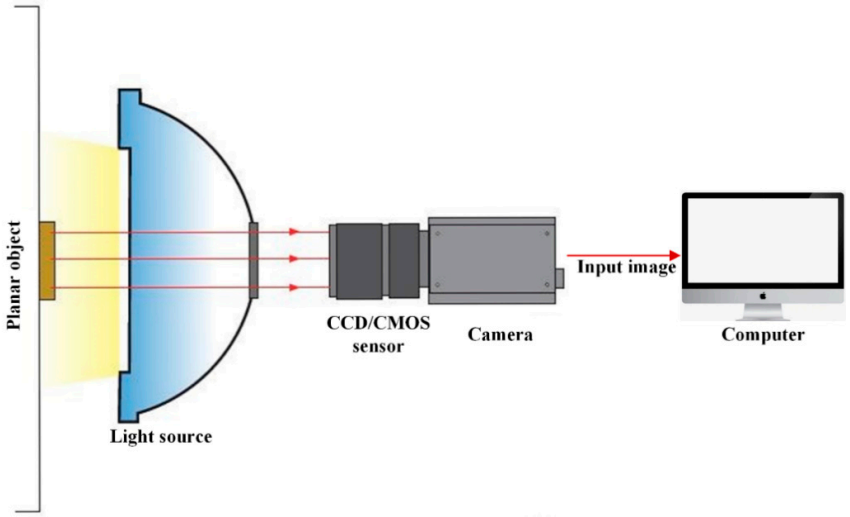

Figure 6. Traditional DIC measurement device.

2.2.2. Laser Beam Position Sensor

In addition to the displacement and strain of the battery pack, to facilitate more accurate analysis, it is also necessary to detect the curvature of the battery pack. In 1989, Scarmino et al. [32] used the Stoney equation to construct the LBPD (Laser beam position detector) to measure the curvature evolution of electrodes during various electrochemical reactions. The principle of curvature detection is shown in Figure 7. The He-Ne laser generator emits a laser beam that is directed towards a beam reflector. The laser beam is then split into two beams by a beam splitter. One beam is directed towards a position detector, while the other beam is directed towards the lower end of the thin film working electrode. The reflected beam passes through the beam splitter and is also directed towards the position detector. The different positions of the two incident beams on the detector generate a linearly proportional differential signal, which is used to calculate the deflection angle θ. Based on the Stoney equation, the stress variation in the thin film working electrode can be derived.

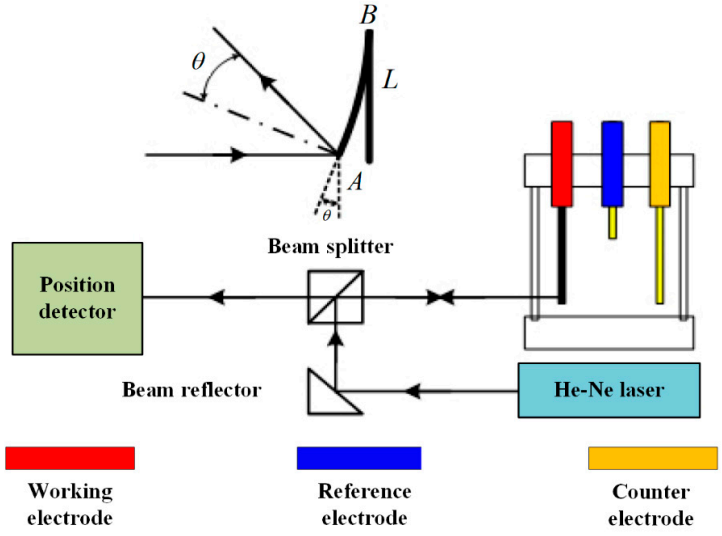

Figure 7. LBPD detection principle [24].

Rosolen et al. [33] used a laser beam detector to study the insertion of Li ions into a membrane electrode and found that the volume change in the non-porous electrode, the surface force, and the presence of a passivation layer in the porous electrode were the main causes of the stress evolution. During electrochemical cycling, Pyun et al. [34] used the laser beam deflection method combined with cyclic voltammetry, the galvanostatic intermittent technique, and the galvanostatic transient technique to observe the growth of membrane $LiCoO_2$ electrodes during lithium ion transport in a three-electrode battery and detect whether stress occurs (which it did). Tavassol et al. [35] immersed Au and Li metal electrode materials in different electrolytes and found that residual tensile stress was observed after delithiation, and its magnitude increased with the increase in the lithiation/delithiation cycle. The results showed that the surface oligomers formed by carbonate solid electrolyte have an effect on the electrode stress evolution. Chung et al. [36] observed the phase transition of $LiMn_2O_4$ electrodes using the in situ laser probe beam deflection technique as evidence of the Jahn–Teller effect above 3 V on the surface of thin film electrode particles.

2.2.3. Multi-Beam Stress Sensor

Generally, when the LBPD technology detects the battery pack, mechanical vibration will affect its accuracy. Chason [37] proposed a multi-beam method MOSS (Multi-beam optical stress sensor) based on Stoney theory to obtain film stress. This technology can be used to measure the stress evolution of film objects. If two beams are irradiated at different positions on the substrate or thin film, the distance between them will vary with the change in sample curvature, and the curvature radius is related to this distance. To address this issue, a standard device with highly reflective and parallel surfaces, such as an optical collimator, is used to form a linear array of multiple beams. These multiple beams irradiated on the sample are parallel and have nearly uniform intensity. The corresponding reflected beams are imaged on a CCD detector. This detector converts the optical signals into electrical signals acquired by a computer. The stress accuracy of the sample depends on the beam spacing. Typically, for in situ cathode stress measurement using MOSS, a battery sample consists of a working electrode (cathode), a lithium foil counter electrode, a separator, and an electrolyte. An optical window allows the laser beam to pass through to detect cathode stress changes. The principle of detection is shown in Figure 8.

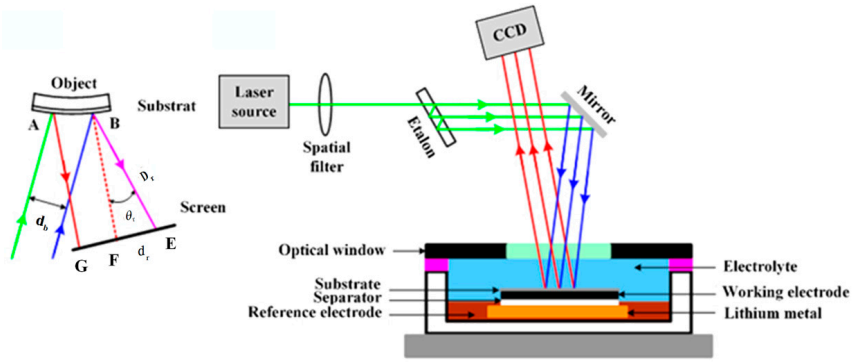

Figure 8. MOSS experimental detection principle [37].

Mukhopadhiyay et al. [38,39] first found that only moderate in-plane compressive stresses of −250 MPa were generated during the galvanostatic cycling of thin film "graphite" electrodes. These stresses were more than an order of magnitude lower than expected and would favor longer cycle life. The novel carbon films with different graphene layer orientations were then investigated as electrode materials for Li-ion batteries, and it was shown that engineering the crystallographic orientation using graphene layers oriented perpendicular to the surface significantly changes the stress evolution during Li insertion. Sethuraman et al. [40,41] applied MOSS to study the dimensional changes associated with electrical cycling of Li-ion batteries. They performed in situ measurements of the biaxial

Young's modulus of Si thin film electrodes as a function of Li concentration. During the intercalation/deintercalation process, elastic stresses are generated as a function of SOC. Nadimpali et al. [42] studied the stress evolution of dry graphite anodes or nickel-cobalt-manganese (NMC) cathodes impregnated with electrolytes. Electrode stress can be induced not only by the Li-ion concentration but also by the applied discharge or charge rate. The above mentioned external sensors of the battery pack using optical technology can only be used to characterize the measurement and estimation of electrodes or single cells and cannot be integrated into commercial battery management systems.

Sensors based on external battery detection can be classified into three main types. We conducted an analysis on their detection methods, advantages, and disadvantages, and the following table lists the relevant research papers related to these sensors. As is shown in Table 2.

Table 2. The literature on sensors based on external batteries.

Sensor	Type	Advantages	Disadvantages	Documents
DIC	displacement measurement	Low-cost equipment.	1. High-cost numerical calculation. 2. Electrode stress measurement is difficult.	[26–31]
LBPD	displacement measurement curvature measurement	1. Can obtain global electrode stress evolution. 2. Strong data processing.	1. High-cost equipment. 2. Electrode stress measurement is difficult.	[32–36]
MOSS	displacement measurement curvature measurement StressAnalysis	The average stress across the electrode can be calculated.	Stresses such as temperature and ion concentration need to be distinguished.	[37–42]

2.3. Battery Module Multi-Sensor Fusion

Integrating multiple types of sensors inside and outside the electric vehicle battery [43] can simplify or improve its management and control, thus providing more possibilities for a more practical, safe, and reliable battery management system. The battery sensor fusion application is shown in Figure 9.

Lee et al. [44] applied MEMS technology to flexible substrates and developed a flexible three-in-one microsensor that can withstand the harsh environment inside lithium batteries and can instantly measure the internal temperature, voltage, and current of the battery. The flexible substrate of this three-in-one microsensor is a 50 μm thick polyimide (PI) foil; the foil is cleaned with acetone and methanol, Cr (500 A) is evaporated by an electron beam evaporator as an adhesion layer, and Au (2500 A) is used as an adhesive layer (sensing layer, as shown in Figure 10(1),(2). The unnecessary Au/Cr film was removed by wet etching to complete the layout structure of the microsensor, as shown in Figure 10(3),(4). Finally, polyimide 7505 was spin-coated on the sample as an insulating layer. The voltage and current probes and the sensor pad terminals are exposed again by employing photolithography to complete the flexible three-in-one microsensor [45], as shown in Figure 10(5),(6).

Ge Lei et al. [46] announced a new energy vehicle lithium-ion battery thermal runaway monitoring and alarm sensor device. In the first operation mode of the device, the temperature sensor, air pressure sensor, and CO gas sensor are in a resting state, and only the VOC gas sensor is in a working state. When the VOC gas sensor detects the electrolyte gas volatilized from the battery due to liquid leakage and other reasons and the concentration reaches the warning threshold, a first-level alarm is generated, and the unit switches to the next operating mode. In the next operating mode, the VOC gas sensor continues to operate. The device utilizes the high-sensitivity characteristics of the VOC gas sensor, has high temperature resistance in lithium-ion battery safety monitoring, and can generate early detection and an alarm for lithium-ion thermal runaway.

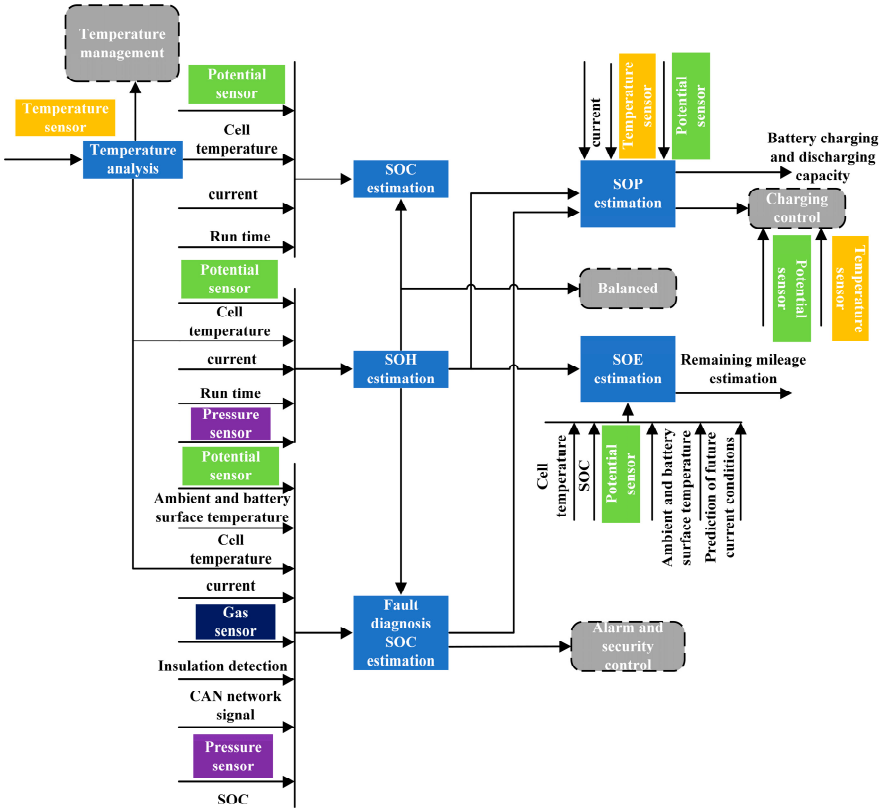

Figure 9. Application of multi-sensor fusion in battery system.

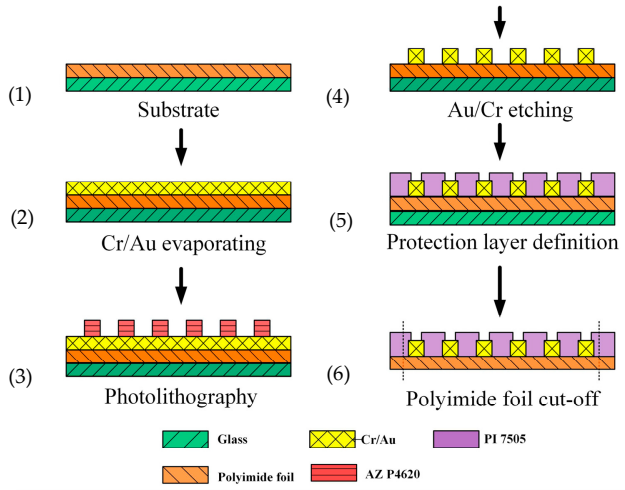

Figure 10. Flexible three-in-one microsensor [45].

3. Research Progress on Sensors for Motor Thermal Management Systems

Many reviews published in recent years have summarized the sensors commonly used in electric vehicle motor modules. Traditional detection includes temperature sensors, infrared thermal sensors, and fiber optic probe sensors [47]. In addition, the application of microcomputer technology has made progress in motor temperature detection, equipment structural changes, performance improvement, and functional expansion. Therefore, scholars worldwide have proposed various motor temperature rise models based on the analysis of the motor thermal circuit model [48]. The technology is integrated into the temperature rise model, and the corresponding temperature detection algorithm is derived, and then the motor temperature rise monitoring algorithm and parameter control rules are stored in the microprocessor to realize the real-time detection of the motor temperature rise. No

position sensor has become the current research hotspot. They are applied to various parts of the motor module to detect various indicators and prevent losses caused by thermal runaway of the motor [49]. Therefore, this paper summarizes the main detection sensors based on the motor module into the following categories: the traditional sensor detection of the motor module and the detection of the motor module without a position sensor. This section introduces the application status of a few commonly used motor detection sensors in the field of motor thermal management. In order to better sort the existing literature, the introduction of the research status is mainly carried out from the perspective of the main problems addressed by the literature and the improvement methods.

3.1. Motor Module Conventional Sensors

The traditional method of motor temperature detection involves embedding the temperature sensor inside the motor and obtaining the temperature parameters via direct measurement. At the same time, infrared thermal imaging technology and standard thermal sensor combined with wireless or slip ring signal transmission technology can also obtain the motor temperature, but this requires additional hardware costs and causes defects in the motor structure. The application range [50] is currently small.

3.1.1. Contact Sensor

Regarding contact temperature measurement in motors, Shen Biaozheng et al. [51] embedded temperature sensors inside the motor to detect the temperature of the rolling motor and constructed a temperature monitoring system for the rolling motor to monitor the approximate motor temperature. However, the monitoring results were greatly affected by the electromagnetic interference of the motor. At the same time, more adhesives were used to fix the probe and the circuit, affecting the heat dissipation of the motor. The sensor also increases the hardware costs. Zhu Hai and Wang Ruihai et al. [52,53] also used buried temperature sensors to monitor the motor temperature. The difference was that they used sensors with better anti-interference performance to improve the reliability of temperature monitoring. Yang Rui [54] designed a series of motor temperature monitoring system based on piezoelectric energy harvesting and power supply. By converting vibration mechanical energy into stable electrical energy, the motor temperature monitoring system was meant to consume less energy; however, embedding temperature sensors to measure the temperature remained most essential. Zhang Zhenhan [55] embedded a Pt100 temperature sensor on the motor rotor and developed a motor rotor temperature measurement device by using slip rings and infrared light pulses to transmit temperature signals, i.e., Zhenhan developed a set based on slip ring signal transmission, which is know as The motor rotor multi-point online temperature measurement device and the motor stator and rotor temperature measurement two-in-one complete machine temperature measurement system.

Huang Yaoqun et al. [56] embedded the thermistor temperature sensor on the rotor of the synchronous motor and used encoded infrared light waves as the temperature transmission method of the rotating part and the static part while also encoding the humidity signal of the sensor through a single-chip microcomputer to eliminate electromagnetic interference to achieve accurate and reliable signal transmission. Feng Yutian et al. [57] monitored the rotor temperature online by measuring the excitation voltage and excitation current while also using infrared light as the signal transmission method to verify the reliability of data transmission by experiment. When Ren Penghui et al. [58,59] studied the temperature measurement method of the three-machine rotating excitation synchronous generator rotor, they improved the slip ring signal transmission mode and connected an independent brush wet current in series with each pole brush circuit. By connecting an independent brush wet current source in series with each pole brush circuit and continuously applying a 30 A DC current between the two brushes, the brushes and slip rings are in reliable contact, ensuring the accuracy of measurement results. Chen Wenzhen et al. [60] designed a Bluetooth-based data transmission system to transmit the signals collected by the temperature sensor to realize the temperature measurement and display of the

motor rotor while also considering the corresponding problems (the fact that the data acquisition is susceptible to electromagnetic interference and the cable connection is complicated). Wu Qiufang and Feng Jianqin et al. [61,62] designed a wireless network-based signal transmission method and a signal transmission method based on mobile communication technology to transmit the signal of the temperature sensor to realize the online monitoring of the motor rotor temperature and finally verified the reliability and stability of the system through experiments. Sui Mingfa [63] used data fusion technology to analyze and process the collected motor temperature data when optimizing the motor temperature measurement system, which improved its accuracy and reliability.

3.1.2. Non-Contact Sensor

Regarding non-contact temperature measurement in motors, researchers are currently focusing on infrared temperature measurement technology. Zhao Xiaodan et al. [64] accurately measured the temperature of the rotor surface by measuring the infrared energy radiated by the rotor of the motor according to the size and wavelength distribution of the infrared radiation energy of the object and the relationship between the surface temperature. The resulting system can draw a temperature distribution map on the surface of each magnetic pole. It is free from electromagnetic field interference and has high sensitivity. It can detect local hot spots of the motor rotor with an accuracy of 0.05 °C. Wu Bo et al. [65] studied the influence of motor rotor rotation and vibration on infrared temperature measurement. In the experiment, a thermocouple contact temperature measurement method was introduced to compare and verify the accuracy of infrared temperature measurement. The influence of the temperature measurement system is very small, and the response of the entire temperature measurement system to the rotor temperature is relatively high, which can meet the temperature measurement requirements of the motor rotor. Liu Junyu [66] analyzed the attenuation of velocity characteristics of infrared thermal devices. In order to reduce the impact of velocity changes on the output, the accuracy of the detector was ensured by means of multi-level differential compensation. At the same time, to address the electromagnetic interference in the process of infrared temperature measurement, the infrared thermal sensor is equipped with a metal shell for electromagnetic shielding to avoid electromagnetic field interference in the signal transmission process. Based on the reversible demagnetization characteristics of the permanent magnet synchronous motor, Zhu Weiguang [67,68] established the relationship between the winding back EMF of the permanent magnet synchronous motor and the temperature of the permanent magnet and measured the winding back EMF through experiments to calculate the average temperature of the permanent magnet. In general, contact temperature measurement has relatively high requirements for signal transmission, and temperature signals need to be transmitted through slip rings or wireless transmission. When the slip ring is used as part of a signal transmission method, there is interference from the slip ring resistance to the signal. Wireless transmission, including Bluetooth, infrared light pulse signal, mobile communication network, etc., will be subject to electromagnetic interference when operating the motor, so the interference factors in the signal transmission process can be reduced. This is a focus point of the research on contact temperature measurement. The infrared temperature measurement technology of the non-contact temperature measurement method is also a contemporary research hotspot, and various researchers are devoting their time to try to improve the resolution, accuracy, and anti-interference ability of the infrared temperature measurement method.

3.2. Motor Module without Position Sensors

The traditional sensor measurement cannot fully reflect the internal temperature of the motor, while the temperature estimation method without a position sensor realizes the observation of the motor temperature through an algorithm, which has broad application prospects and is more favored by researchers. After nearly two decades of research, the temperature estimation method [69] has only been developed recently. At present, it is

mainly divided into two types: the temperature estimation method based on the motor thermal model and the temperature estimation method based on the stator resistance identification. Each method also has several ways of implementation, as shown in Figure 11.

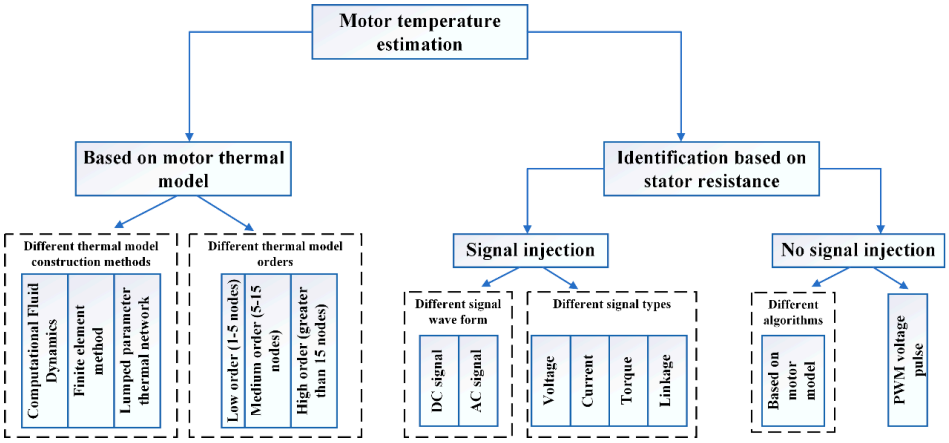

Figure 11. Motor temperature estimation method.

3.2.1. Thermal Model Temperature Detection

Inside the motor, heat is transferred in three ways: conduction, convection, and radiation. By analyzing the heat distribution of the motor, a motor thermal network model can be constructed [70], and then high-resolution motor temperature distribution information can be obtained. To realize the motor temperature estimation, the thermal model method is based on this principle. The motor thermal model is composed of many thermal nodes representing the temperature of different regions, and each node is connected by the thermal conductance—which completes the heat conduction and convective heat transfer—and the thermal capacitance associated with each node, which considers the heat storage effect. By analyzing the thermal network loss, thermal conductance, thermal capacitance, and boundary cooling conditions, the temperature value of each node can be obtained and the motor temperature estimation can subsequently be realized. Nategh et al. [71] used computational fluid dynamics and finite element analysis methods [72] to build a thermal model of the motor, which can provide effective predictions for system operation. However, these two methods require a large amount of computing resources during operation, which is not conducive to real-time temperature monitoring. To solve this problem, Shafigh et al. [73,74] proposed a modeling and analysis method based on the transient thermal effect of the motor, using computational fluid dynamics to model the air flow in the motor and input the heat transfer boundary. The developed thermal model combines finite elements and lumped parameters, and due to the relatively small scale of the model, the defect of slow running speed can be overcome. Compared with the two above-listed methods, the lumped parameter thermal network model requires less computation and can meet the needs of real-time temperature estimation. This method is the most widely used in motor temperature monitoring and thermal protection. As shown in Figure 12a,b, assuming the experimental motor has axial symmetry, the heat sources in each component are uniformly distributed. In terms of heat transfer, only the axial heat transfer in components such as the shaft, casing, and permanent magnet is considered. When establishing the thermal network model, the thermal resistances of each component are connected, taking into account the heat sources and heat capacitance. By establishing this thermal network model, the temperature distribution and thermal coupling effects of the motor can be analyzed under different operating conditions. This helps one to understand the heat exchange between internal components of the motor, optimize heat dissipation design, and improve thermal management capability.

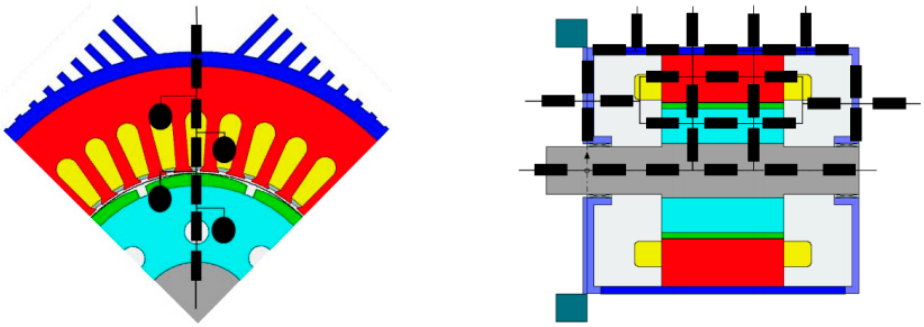

(**a**) (**b**)

Figure 12. Thermal network model of permanent magnet synchronous motor.

It should be noted that this is a simplified model that involves certain assumptions and ignores other possible heat transfer paths and influencing factors. In practical applications, more detailed and accurate thermal analysis and modeling should be conducted based on specific circumstances.

When constructing the thermal model of the motor, it is also necessary to fully consider the design requirements and determine the order of the thermal model. Some of the existing literature realizes the construction of thermal models based on basic physical knowledge and complex heat exchange theory. The main thermal path of the motor is simulated by the low-order (2–5 nodes) thermal mesh, and the thermal parameters in the model are obtained by experimental training. Other parts of the literature [75,76] analyze the modeling of important components in the motor at a lower local discrete level based on heat transfer theory and when the model order is in the range of 5 to 15 nodes. The calculation of the thermal model parameters is mainly based on the motor material and geometric data, and it can also be optimized based on experience, which is beneficial to reduce the calculation requirements; however, the estimated temperature is the average temperature of the device and therefore cannot reflect the temperature information of a specific node. For the extremely critical and important devices in the motor, a higher level of discretization is set during modeling. In this paper, finer grids are set relative to the coordinate system so that an accurate thermal model of the motor can be obtained, and at the same time, it can be estimated that the motor is different. The node temperature at the position [77] will inevitably lead to a sharp increase in the order of the motor thermal model [78], increasing the difficulty of calculation. In addition, many scholars have extended the application of lumped parameter thermal network models. Wallscheid [79] constructed a low-order lumped parameter thermal network motor model based on four nodes of the stator yoke, stator teeth, stator windings, and permanent magnets and determined the thermal network parameters of the motor through the particle swarm optimization algorithm combined with experimental data, taking into account variable parameters and physical constraints and expanding the scope of application of the model. In order to reduce the complexity of the model and the number of temperature sensors, Kral et al. [74] simplified the lumped parameter thermal network model so that it required only two time constants and one temperature sensor located in the stator core, thereby omitting the motor coolant volume and flow parameters. The model is based on average zone temperatures so that hot or cold spot information is not considered. Demetriades et al. [80] relied on the geometric structure of the motor to obtain the parameters of the real-time thermal model and performed the discretization in the form of state space to reduce the order and complexity of the thermal model. Jiang et al. [81] considered the frequency change and analyzed the effect of frequency change on eddy current loss, hysteresis loss, and harmonic current loss to realize the thermal protection of the motor in the full speed range.

Kylander [82] studied the more widely used motor lumped parameter thermal model and gave the steady-state and transient solution of the motor temperature for this model. Andersson [83] gave two simplified thermal models of permanent magnet synchronous

motors, one based on actual physical parameters and the other based on optimized parameters. Boglietti et al. [84] conducted extensive studies on the key parameters that determine the thermal model of the motor, including the equivalent thermal resistance between the motor housing and the environment, the interface gap between the laminations and the housing, and the heat transfer between the windings and the end shields. Coefficients and other parameters are used to improve the accuracy of the motor temperature estimation. Seong [85] considered the influence of load, established the second-order fitting power loss distribution model of the motor in the constant torque operating range by using the experimental design and response surface method, and used the equivalent thermal resistance model to calculate the temperature rise of the motor. Martinez-Botas [86] introduced an improved thermal model method, which builds a motor thermal model based on temperature measurements and experiments, and then combines the recursive parameter estimation method to realize motor thermal condition monitoring. Xiao et al. [87] used the AVL test system to build a motor temperature rise test bench to verify the estimation accuracy of the rotor temperature estimation model based on magnetic–thermal bidirectional coupling under different ambient temperatures and different operating conditions. The actual rotor temperature during motor operation is obtained and compared with the model-estimated temperature to validate and optimize the thermal network model to improve its temperature estimation accuracy. The measurement principle is shown in Figure 13.

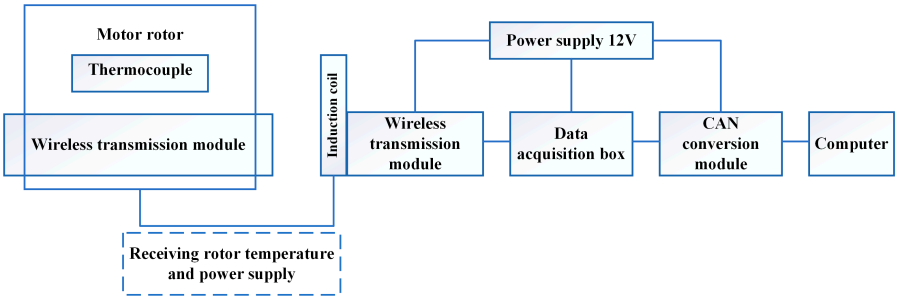

Figure 13. Measuring principle of motor temperature rise.

Zhang [88] proposed a transfer function method considering the material temperature characteristics and heat transfer coefficient, introduced Green's function as a new transfer function to build a motor thermal model, and realized the calculation of the average temperature and node temperature of the motor.

3.2.2. Signal Injection Temperature Detection

The above thermal model method estimates the motor temperature based on the motor thermal parameters, which has no negative effect on the motor operating performance and is an attractive temperature monitoring scheme. However, when constructing a motor thermal model, it is often necessary to assume that the selected system is a thermally stable system and that changes in motor parameters or cooling conditions cannot be updated in real time, meaning that the thermal model parameters must be updated offline, which will greatly affect the accuracy of temperature estimation. In addition, the accuracy of thermal parameter identification and the loss calculation results both affect the reliability of the thermal model. Differences in the parameter identification results can lead to huge temperature estimation errors and negatively affect the temperature estimation results. Compared with the thermal model method, the signal injection method has higher robustness and is insensitive to changes in the cooling capacity and working state of the motor, resulting in it being favored by researchers worldwide. The signal injection method can be integrated into the existing motor control strategy, and the required signal injection is realized by the motor controller so that no additional hardware equipment is required, the operation is simple and easy to implement, and extremely high application value is ensured. In 1980, Derek A. Paice [89] first proposed DC injection technology, which is

used to inject a very small DC signal into the stator phase winding and calculate the stator resistance by measuring the DC component of the stator voltage and current. Through the stator resistance, the relationship between it and its temperature enables motor temperature estimation. The system control block diagram of the temperature estimation algorithm for a Permanent Magnet Synchronous Motor (PMSM) with DC voltage injection is as follows: In this method, a DC bias voltage is injected along the α-axis. The injected voltage goes through Space Vector Pulse Width Modulation (SVPWM), which introduces DC voltage and current components into the motor phase windings. The DC component of phase A current is sampled, and together with the injected voltage, it is used in calculations to obtain an estimated value of the stator winding temperature. As is shown on Figure 14.

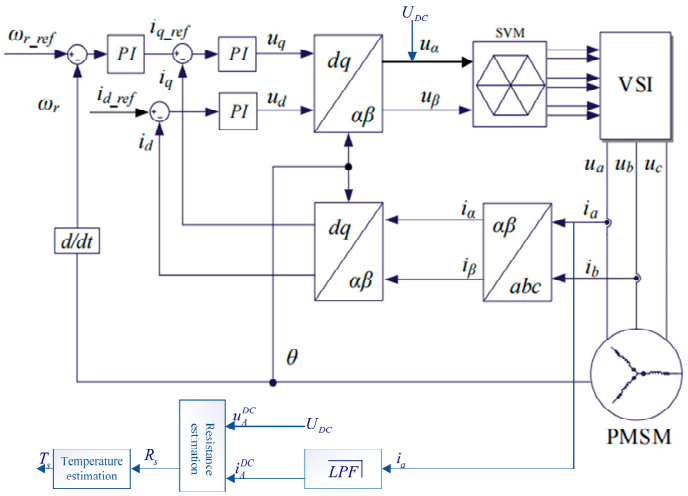

Figure 14. System control block diagram based on DC voltage signal injection.

On this basis, DC signal injection technology is applied to the soft start induction motor, the existing DC signal injection technology is improved, and a simplified signal injection technology is proposed, that is, the insulated gate bipolar transistor (IGBT) is turned on and off to realize the injection of DC voltage bias signal to reduce the torque ripple and magnetic saturation problems caused by continuous signal injection. However, for the above DC signal injection strategy, although the resistance identification accuracy and robustness are high, an additional signal injection device needs to be installed, which increases the volume and cost of the system [90,91]. In response to the above problems, Zhang et al. [92] proposed to apply the signal injection technology to the variable frequency speed control motor and realize the required signal injection through the inverter so that there is no need to install additional signal injection devices. Cheng et al. [93] discussed at length the effect of the non-ideal characteristics of the inverter on the extraction of the DC voltage signal and proposed several compensation techniques to achieve a consistent estimation of the stator resistance. Aiming to solve the problem regarding the fact that the DC component of the voltage and current generated by the injected signal is small (which is not conducive to the accurate extraction of the signal), a real-time signal processing technique is also proposed in this paper, i.e., the DC component can be accurately extracted by filtering with a digital notch filter and a low-pass filter, respectively, to improve the accuracy of temperature estimation. The above-listed DC signal injection method can effectively estimate the motor temperature, but it is not suitable for monitoring the temperature of high-power motors.

For high-power motors [94], the resistance value of the stator resistance is often extremely small, so the amplitude of the DC component of the voltage generated by the injected DC signal on the phase winding is also very small (relative to the peak value of the phase AC voltage), and the extraction of the DC voltage components is difficult, affecting the accuracy of the resistance identification and temperature estimation results. When a large signal is injected, the amplitude of the output torque ripple increases, which affects the performance of the motor. It is difficult to ensure high temperature estimation accuracy

and normal operation of the motor at the same time. Therefore, the above signal injection strategy still needs to be continuously improved to meet the temperature estimation requirements of high-power motors. Compared with DC signal injection technology, AC signal injection technology can also be used for motor temperature estimation. The system control block diagram of the temperature estimation method based on AC current injection technology is shown in Figure 15. In this method, an AC current signal is inputted into the d-axis of the dq coordinate system. Through motor vector control, DC components of voltage and current are generated in the stator windings of the motor. The DC components of the voltage and the DC components of the phase current are sampled separately. The temperature estimation value is obtained based on the formula.

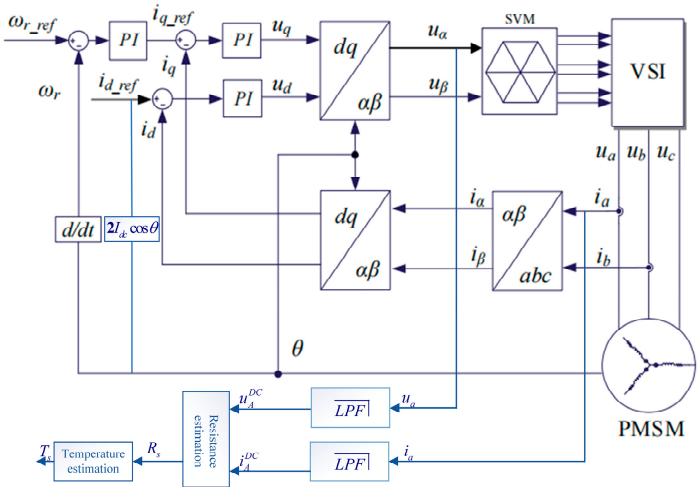

Figure 15. System control block diagram based on AC injection method.

In terms of the motor closed-loop control system, Wilson et al. [95] proposed to realize the superposition of the DC signal on the stator winding by injecting the AC signal in the d-axis and gave two calculation techniques of the fixed "angle" and fixed "amplitude" of the stator resistance. At the same time, two injection signal extraction methods, unipolar and bipolar, are described, and the window function is used to reduce the voltage harmonics when the current changes to achieve a smooth transition. Reigosa et al. [96,97] used low and high frequency signal injection to realize stator resistance identification, in which the change in motor parameters (speed, inductance, etc.) greatly affects the resistance identification results, and the resistance identification accuracy is also affected by attention. The influence of the frequency of the input signal will affect the accuracy of the motor temperature estimation. For motors using the direct torque control strategy [98], a torque signal injection strategy is proposed, which involves injecting a DC torque signal into the torque control loop and realizing the DC current signal on the phase winding via direct torque control. After superposition, the resistance identification and motor temperature estimation are realized, and the quantitative relationship between the DC offset and the corresponding torque change is also given. Zhang et al. [99] implemented the injection of high-frequency current signals by applying an external high-frequency torque signal to the hysteresis torque control of the motor drive, and then completed the stator temperature estimation. In addition, He et al. [100] proposed the use of DC flux injection technology to realize the thermal monitoring of direct torque control motors, derived the quantitative relationship between the desired injected current and flux compensation, and then superimposed the flux linkage in the flux linkage control loop bias signal for current injection. Zhang [101] used high-frequency rotating flux injection technology to realize stator resistance identification and motor temperature estimation.

At present, the signal injection strategies all face the same problem in the implementation process, i.e., the signal injection leads to output torque ripple, increases copper consumption, and affects the performance and efficiency of the motor. To this end, re-

searchers have conducted in-depth research on the above issues, achieving the following outcomes. Aiming to alleviate the torque ripple caused by signal injection, He et al. [102] proposed a torque ripple compensation method, which involved compensating the torque ripple by injecting additional second harmonic current in the vector control, thereby reducing the output torque. However, injecting an additional harmonic current will inevitably lead to increased copper loss and reduce the operating efficiency of the motor. At the same time, based on flux linkage injection technology [103], the opposite pulsating torque is generated by injecting the second harmonic flux linkage in the direct torque control to compensate for the low-frequency pulsation generated when the signal is injected and reduce and eliminate the torque pulsation purpose. Wang et al. [104] introduced a real-time motor parameter identification method based on variable frequency signal injection without generating additional torque ripple. However, there is no evidence that this method can be used for motor thermal monitoring because there is no guarantee that the accuracy of the stator resistance identification can meet the temperature estimation requirements. For direct torque control motors, torque and flux injection techniques are used to estimate the stator temperature, and at the same time, to reduce the extraction error of the DC voltage and current components, the duty cycle and terminal voltage are estimated, respectively [105].

For small and medium size motors, Huang et al. [106] proposed an equivalent winding model and considered the influence of filling factor and void ratio on the temperature rise of the motor to reduce the temperature estimation error. Wallscheid et al. [107] analyzed the advantages and disadvantages of the thermal model method and the signal injection method in detail, and on this basis, proposed the fusion of two methods to improve the accuracy and robustness of temperature estimation, mainly through the Kalman filter. The goal of accurately estimating motor temperature is achieved by combining a lumped parameter thermal network model and a motor model-based temperature observer. The bus current impact and torque ripple caused by signal injection have been studied in depth, respectively. Lu et al. [108] proposed a nonlinear control method to suppress the torque ripple. In addition, Zhang et al. [109] analyzed the magnetic saturation problem caused by DC signal injection in detail, determined the magnetic saturation phenomenon that the injected signal will change during the motor operation cycle, and analyzed the effects of magnetic saturation on the motor current, motor thermal performance, stator winding resistance, and temperature, highlighting that magnetic saturation has no effect on stator resistance and temperature estimation performance and demonstrating the feasibility of implementing the aforementioned active thermal management technique based on motor temperature estimation under different load conditions. Sun Jiayu [110] combined the heat source acquisition model based on the signal injection method with the motor temperature identification model based on the thermal network method, and at the same time, considered the coupling relationship between motor parameters and temperature and finally increased the temperature of the stator winding of the permanent magnet synchronous motor. Figure 16 is a thermal path diagram of the stator winding in the axial direction. The stator winding is divided into 20 layers in equal proportions, with each layer consisting of wire, wire insulation, and impregnation in parallel. Finally, the winding is equivalent to a radial $\times$ axial arrangement, with 10 $\times$ 20 units, and the heat sources are evenly distributed among each unit. The considerations for the end-winding are the same as those for the winding inside the slots. The newly constructed stator winding model remains in the same position in the thermal network model, and the corresponding components connected to it are also discretized accordingly. The degree of discretization decreases gradually with the distance from the stator winding.

The above research results have reduced the influence of torque ripple to a certain extent and promoted the application of signal injection strategy and even temperature estimation theory; however, the scope of application is limited, and the optimal setting of signal injection strategy remains an important issue to be analyzed, discussed, and resolved. Overall, the existing literature contains in-depth and extensive research on the motor temperature estimation method, which reflects the feasibility and advantages of the

temperature estimation method. The aforementioned researchers laid a solid foundation for the development of this paper. However, the existing motor temperature estimation methods have certain limitations and face a series of problems with regards to practical application. Therefore, it is necessary and practical to conduct further research on the temperature estimation strategy.

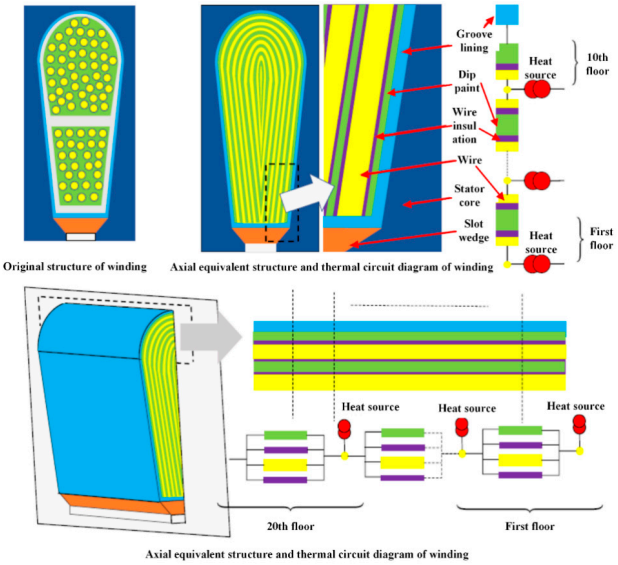

Figure 16. Equivalent schematic diagram of motor stator winding [110].

Sensors based on electric vehicle motor detection can be divided into four main types. We conducted an analysis on their detection methods, advantages, and disadvantages, and the following table lists the relevant research papers related to these sensors. As is shown on Table 3.

Table 3. The literature on motor-based sensors.

Method	Advantages	Disadvantages	Documents
traditional contact sensor	1. Small in size, anti-electromagnetic interference.	1. The wiring and transmission is complicated. 2. Difficulty in installation and maintenance.	[51–63]
Traditional Non-Contact Sensors	2. Non-conductive, chemically inert.	1. Reliability, low-resolution, high-cost.	[64–68]
thermal model	1. A lumped parameter thermal network model can be constructed to obtain high-resolution motor temperature distribution information.	1. Changes in motor parameters or cooling status cannot be updated to the thermal model in real-time 2. Need to install temperature sensor.	[70–88]
signal injection	1. Temperature estimation can be realized by injecting voltage, current, torque, or flux linkage signals.	1. The accuracy of resistance identification is greatly affected by the injection signal. 2. It is easy to affect the output torque of the motor.	[89–110]

4. Research Progress on Sensors for Air-Conditioning Thermal Management System

A recent review of automotive air conditioning sensors [111] summarizes the differences in sensor applications between automatic air conditioning and electric air conditioning, which usually includes several sensors: temperature, pressure, and air volume. However, there are also some differences, such as the sunlight in the automatic air conditioner, the suction type in the car, the air quality, and the use of defogging sensors. Therefore, this paper sorts the applications of automotive air conditioning sensors into the following categories: evaporator sensor applications, compressor sensor applications, and multi-sensor fusion for air conditioning systems [112]. This section introduces the application status of three types of system sensors in the field of electric vehicle air conditioning. In order to better sort the existing literature, the introduction of the research status is mainly

carried out from the perspective of the main problems addressed by the literature and the improvement methods.

4.1. Evaporator Temperature Sensor

The evaporator temperature sensor is arranged on the evaporator of the automotive air conditioning system to detect the temperature change and temperature signal on the surface of the evaporator and convert it into an electric signal and input it to the ECU (Electronic Control Unit) of the air conditioning control system. After comparing the input temperature signal with the set temperature adjustment signal, control the on-off of the electromagnetic clutch of the air conditioner compressor to control the operation of the compressor and use this sensor to detect the temperature signal to prevent the evaporator surface from frosting phenomenon [113]. Bao et al. [114] studied the position of the temperature sensor on the evaporator and found that the position of the temperature sensor should be selected when the position reaches 3 °C, the highest temperature is above 0 °C, and the lowest temperature is below 0 °C. Additionally, 20~25% of the surface of the evaporator begins to freeze at the best position. Yang et al. [115] analyzed the effect of frost on the surface of the air conditioning evaporator on the cooling performance and further optimized the temperature sensor position and control parameters (cut-off/connection temperature). The results of the automotive environment simulation test show that, after optimization, the average temperature of each air outlet of the air conditioner is reduced by 1.7–2.7 °C, and the cut-off frequency of the compressor is reduced by 79%. After Cai et al. [116] reduced the original range of evaporator temperature control parameters to −1~2 °C, the phenomenon of frequent starting and stopping of the air conditioner was solved. Dong et al. [117] studied the variation of heating capacity and outlet air temperature of the horizontal and vertical sensor arrangement of the evaporator under highly cold, high humidity, and cold humidity conditions, and the performance of the horizontal arrangement structure under the frosting condition was observed to be better than the vertical arrangement structure. When studied as a condenser, there is less difference in performance between the horizontal and vertical sensor arrangement.

4.2. Compressor Temperature and Pressure Sensor

The compressor is the core component of the automotive air conditioning system. It is mainly responsible for compressing the liquid into a high-temperature, high-pressure gaseous state to perform a refrigeration cycle. Huang et al. [118] proposed a performance test study based on the thermal balance of the compressor. When the temperature sensor is used alone in the field environment, the relative error is less than 10.2%. When the pressure sensor + temperature sensor are used together, the relative error is less than 8.4%. This proves that the combined use of temperature and pressure sensors has a good effect on compressor testing. Overheating damage is a great danger in compressor operation. Generally, the discharge temperature sensor is used to protect the compressor from overheating. Wu et al. [119] adapted the discharge temperature sensor to the top cover of the compressor and began to optimize the protection trigger mechanism for insufficient refrigerant flow to prevent the compressor from experiencing damage from overheating. He et al. [120] investigated the operation mechanism and efficiency of the compressor under the incomplete superheat cycle. The test showed that the coefficient of performance (COP) of the compressor was reduced at extremely low frequencies, and the drop of the discharge temperature exceeded that of the superheating section by 28.9~40.3%; when operating near the rated frequency, the exhaust temperature drop was only reduced by 0.8~1.3%, and the COP value did not change much. Lu et al. [121] investigated the influence of the position of the compressor temperature and pressure sensor on the compressor overheating. The temperature and pressure sensor were installed at 120 mm from the compressor outlet, and the temperature and pressure sensor were operated at 130 °C, 135 °C, and 145 °C at the exhaust gas for 4 h, respectively. It was concluded that the temperature and pressure sensor should be set at 120 mm, and the influence of overheating below 145 °C is small.

Cao et al. [122] proposed a method of using FBG sensors instead of temperature sensors to monitor the temperature of compressors. The fabricated FBG temperature sensor was placed in a high and low temperature test box for calibration. Through comparison, it was found that the performance of this type of sensor was the same as that of a traditional temperature sensor.

4.3. Multi-Sensor Fusion of Air Conditioning System

The air-conditioning control system design based on multi-sensor information fusion needs to use multiple sensors to collect status information at the same time and realize information fusion in the CPU (central processing unit) of the air-conditioning system. The parallel output multi-channel control information [123] is used to control automotive air conditioning system equipment and then for the the purposes of energy saving and consumption reduction. Liu et al. [124] compared the single-sensor scheme with the multi-sensor scheme and found that the multi-sensor scheme can make the air flow in the air-conditioning area evenly distributed, the relevant personnel feel comfortable, and meet the comfort requirements of the vehicle occupants. Ge et al. [125] further determined a reasonable early start-up period through unary regression analysis based on the multi-sensor fusion of the air conditioning system and then predicted the cooling load of the next day through the BP neural network, calculating the comfort demand and energy consumption demand in advance. analysis. The multi-sensor fusion decision control of the air-conditioning system also brings a lot of uncertainty, and the air-conditioning system with fused information is less robust; the diagnosis of fault information in the multi-sensor fusion system [126] is also a research hotspot at this stage. Usoro [127] used a method based on the fault residual model to diagnose the sudden failure of the temperature sensor. By establishing a nonlinear model and combining it with the Kalman filter, the detection of the sudden fault was achieved. Wang [128] continued this method and proposed a method to estimate the temperature sensor bias of the cold water system based on the residual model and then used the mass and energy conservation relationship to establish a residual equation group to complete the diagnosis. Lee [129] used a method involving an artificial neural network to detect and diagnose the sensor failure of the air conditioning system from the perspective of neural network model identification, proposing the use of the regression model to restore the air supply temperature of the air conditioning box.

5. Conclusions

The use of sensors in monitoring the thermal management system of electric vehicles has proven to be an effective and important approach in mitigating accidents. This article aimed to provide an overview of sensor applications in the field of thermal management for electric vehicles, focusing on recent advancements and analyzing existing methods. The detection methods discussed in this article were categorized into three main groups: battery modules, motor modules, and air conditioning systems.

To begin, the article introduced the fundamental principles behind different types of sensors used in these applications, providing a comprehensive understanding of their working mechanisms and highlighting their significance in ensuring the safe and efficient operation of electric vehicles. Subsequently, the article delved into the current research motivations and solutions, examining various methods from different perspectives. It explored the utilization of temperature sensors, pressure sensors, flow sensors, and other relevant sensors in monitoring and controlling the thermal management system. Each detection method based on different sensors possesses distinct characteristics, which were summarized and highlighted in the article. The advantages and limitations of each approach were discussed, providing insights into their practical implementations and potential challenges. The article also addressed the importance of sensor calibration and validation to ensure accurate and reliable measurements.

Moreover, the article outlined the limitations of traditional sensor detection accuracy and the need for improved stability in advanced sensor detection. It explained the existing

issues and addressed them by proposing improvements in two key areas: system signal preprocessing and sensor model structure. Advanced signal processing techniques, such as noise reduction and data fusion algorithms, were explored to enhance the accuracy and robustness of sensor measurements. Additionally, the development of more sophisticated sensor models that account for dynamic operating conditions and environmental factors was emphasized. Although significant progress has been made in enhancing these detection methods, there are still numerous challenges that need to be addressed. The article acknowledged the complexity of the thermal management system in electric vehicles and the importance of considering factors such as thermal coupling and transient behaviors. The authors emphasize that the development of sensor detection in future electric vehicle thermal management systems remains a prominent point of focus for researchers within the field and that continued advancements in sensor technology and data analysis techniques are crucial for optimizing the thermal performance, energy efficiency, and overall safety of electric vehicles.

Author Contributions: Conceptualization, B.D. and H.W.; methodology, L.Y.; writing—original draft preparation, Y.X.; writing—review and editing, A.C.; All authors have read and agreed to the published version of the manuscript.

Funding: This research received no external funding.

Acknowledgments: In this section, I can acknowledge any support given which is not covered by the author contribution or funding sections.

Conflicts of Interest: The authors declare no conflict of interest.

Abbreviations

FBG	Fiber Bragg Grating
FO	Fiber Optic
SOC	State Of Charge
SOH	State Of Health
BMS	Battery Management System
RTD	Resistance Temperature Detector
TFTC	Thin-film Thermocouple
DIC	Digital Image Correlation
MOSS	Multi-beam Optical Stress Sensor
NMC	Nickel-cobalt-manganese
LBPD	Laser Beam Position Detector
IGBT	Insulated Gate Bipolar Transistor
ECU	Electronic Control Unit
COP	Coefficient Of Performance
CPU	Central Processing Unit
PMSM	Permanent Magnet Synchronous Motor
SVPWM	Space Vector Pulse Width Modulation

References

1. Zhu, Y.; Bai, J. Application Research of Sensor Technology in Electric Vehicle Battery Management System. *Automob. Electr. Appl.* **2021**, 17–20. [CrossRef]
2. Zhao, X.; Wang, P.; Chao, P.; Li, N.; Liang, X.; Dong, H. Research progress of lithium-ion battery safety detection sensors. *Traffic Inf. Saf.* **2022**, *40*, 127–136.
3. Cheng, X.; Pecht, M. In situ stress measurement techniques on li-ion battery electrodes: A review. *Energies* **2017**, *10*, 591. [CrossRef]
4. Ouyang, C.; Liang, B.; Liu, Y.; Lai, Y.; Liu, Y. Research Progress on Thermal Safety of Li-ion Power Batteries. *Power Technol.* **2014**, *38*, 382–385.
5. Yang, G.; Leitão, C.; Li, Y.; Pinto, J.; Jiang, X. Real-time temperature measurement with fiber Bragg sensors in lithium batteries for safety usage. *Measurement* **2013**, *46*, 3166–3172. [CrossRef]
6. Sommer, L.W.; Kiesel, P.; Ganguli, A.; Lochbaum, A.; Saha, B.; Schwartz, J.; Bae, C.J.; Alamgir, M.; Raghavan, A. Fast and slow ion diffusion processes in lithium ion pouch cells during cycling observed with fiber optic strain sensors. *J. Power Sources* **2015**, *296*, 46–52. [CrossRef]

7. Sommer, L.W.; Raghavan, A.; Kiesel, P.; Saha, B.; Schwartz, J.; Lochbaum, A.; Ganguli, A.; Bae, C.J.; Alamgir, M. Monitoring of intercalation stages in lithium-ion cells over charge-discharge cycles with fiber optic sensors. *J. Electrochem. Soc.* **2015**, *162*, A2664. [CrossRef]
8. Fortier, A.; Tsao, M.; Williard, N.D.; Xing, Y.; Pecht, M.G. Preliminary study on integration of fiber optic Bragg grating sensors in li-ion batteries and in situ strain and temperature monitoring of battery cells. *Energies* **2017**, *10*, 838. [CrossRef]
9. Novais, S.; Nascimento, M.; Grande, L.; Domingues, M.F.; Antunes, P.; Alberto, N.; Leitão, C.; Oliveira, R.; Koch, S.; Kim, G.T.; et al. Internal and external temperature monitoring of a Li-ion battery with fiber Bragg grating sensors. *Sensors* **2016**, *16*, 1394. [CrossRef]
10. Meyer, J.; Nedjalkov, A.; Doering, A.; Angelmahr, M.; Schade, W. Fiber optical sensors for enhanced battery safety. In *Fiber Optic Sensors and Applications XII*; SPIE: Bellingham, WA, USA, 2015; Volume 9480, pp. 190–201.
11. Xu, S.; Hu, J.; Xu, C.; Hui, D. A Lithium-ion Battery Temperature Measurement Method Based on Fiber Bragg Grating Sensing. *Electr. Appl. Energy Effic. Manag. Technol.* **2020**, *57*, 85. [CrossRef]
12. Wang, H.; Cao, S.; Su, J.; Xu, H.; Wang, Z.; Zeng, J.; Wei, W. Lithium battery pack temperature field monitoring based on double-clad fiber Bragg grating sensor. *Acta Phys. Sin.* **2022**, *71*, 104207. [CrossRef]
13. Amietszajew, T.; McTurk, E.; Fleming, J.; Bhagat, R. Understanding the limits of rapid charging using instrumented commercial 18650 high-energy Li-ion cells. *Electrochim. Acta* **2018**, *263*, 346–352. [CrossRef]
14. Huang, J.; Albero Blanquer, L.; Bonefacino, J.; Logan, E.R.; Corte, D.A.D.; Delacourt, C.; Gallant, B.M.; Boles, S.T.; Dahn, J.R.; Tam, H.-Y.; et al. Operando decoding of chemical and thermal events in commercial Na (Li)-ion cells via optical sensors. *Nat. Energy* **2020**, *5*, 674–683. [CrossRef]
15. Lee, C.Y.; Lee, S.J.; Chen, Y.H.; Chung, M.Y.; Han, K.C.; Chang, Y.M.; Tang, M.S. In-situ monitoring of temperature and voltage in lithium-ion battery by embedded flexible micro temperature and voltage sensor. *J. Electrochem. Sci.* **2013**, *8*, 2968–2976. [CrossRef]
16. Zhu, S.; Han, J.; An, H.Y.; Pan, T.S.; Wei, Y.M.; Song, W.L.; Chen, H.S.; Fang, D. A novel embedded method for in-situ measuring internal multi-point temperatures of lithium ion batteries. *J. Power Sources* **2020**, *456*, 227981. [CrossRef]
17. Mutyala, M.S.K.; Zhao, J.; Li, J.; Pan, H.; Yuan, C.; Li, X. In-situ temperature measurement in lithium ion battery by transferable flexible thin film thermocouples. *J. Power Sources* **2014**, *260*, 43–49. [CrossRef]
18. Pan, X.; Yang, Y.; Wang, Q.; Zhou, Z.; Li, G. Research on Flexible Thin Film Sensors for In-situ Temperature Monitoring of Lithium Batteries. *Sens. Microsyst.* **2018**, *37*, 27–29. [CrossRef]
19. Martiny, N.; Geder, J.; Wang, Y.; Kraus, W.; Jossen, A. Development of a thin-film thermocouple matrix for in-situ temperature measurement in a lithium ion pouch cell. In Proceedings of the 2013 IEEE, Baltimore, MD, USA, 3–6 November 2013.
20. Martiny, N.; Rheinfeld, A.; Geder, J.; Wang, Y.; Kraus, W.; Jossen, A. Development of an all kapton-based thin-film thermocouple matrix for in situ temperature measurement in a lithium ion pouch cell. *IEEE Sens. J.* **2014**, *14*, 3377–3384. [CrossRef]
21. Zhu, S.; Yang, L.; Wen, J.; Feng, X.; Zhou, P.; Xie, F.; Zhou, J.; Wang, Y. In operando measuring circumferential internal strain of 18650 Li-ion batteries by thin film strain gauge sensors. *J. Power Sources* **2021**, *516*, 230669. [CrossRef]
22. Zhu, S.; Yang, L.; Fan, J.; Wen, J.; Feng, X.; Zhou, P.; Xie, F.; Zhou, J.; Wang, Y. In-situ obtained internal strain and pressure of the cylindrical Li-ion battery cell with silicon-graphite negative electrodes. *J. Energy Storage* **2021**, *42*, 103049. [CrossRef]
23. Jin, Y.; Zheng, Z.; Wei, D.; Jiang, X.; Lu, H.; Sun, L.; Tao, F.; Guo, D.; Liu, Y.; Gao, J.; et al. Detection of micro-scale Li dendrite via H2 gas capture for early safety warning. *Joule* **2020**, *4*, 1714–1729. [CrossRef]
24. Guo, D.; Liu, Y.; Xiao, P.; Sun, L.; Tao, F. Study on early warning parameters for thermal runaway of lithium ion batteries used in energy storage power stations. *Fire Sci. Technol.* **2020**, *39*, 1156.
25. Li, B.; Parekh, M.H.; Adams, R.A.; Adams, T.E.; Love, C.T.; Pol, V.G.; Tomar, V. Lithium-ion battery thermal safety by early internal detection, prediction and prevention. *Sci. Rep.* **2019**, *9*, 13255. [CrossRef] [PubMed]
26. Zhu, S.; Han, J.; Pan, T.S.; Wei, Y.M.; Song, W.L.; Chen, H.S.; Fang, D. A novel designed visualized Li-ion battery for in-situ measuring the variation of internal temperature. *Extrem. Mech. Lett.* **2020**, *37*, 100707. [CrossRef]
27. Chen, J.; Liu, J.; Qi, Y.; Sun, T.; Li, X. Unveiling the roles of binder in the mechanical integrity of electrodes for lithium-ion batteries. *J. Electrochem. Soc.* **2013**, *160*, A1502. [CrossRef]
28. Qi, Y.; Harris, S.J. In situ observation of strains during lithiation of a graphite electrode. *J. Electrochem. Soc.* **2010**, *157*, A741. [CrossRef]
29. Jones, E.M.; Silberstein, M.N.; White, S.R.; Sottos, N.R. In situ measurements of strains in composite battery electrodes during electrochemical cycling. *Exp. Mech.* **2014**, *54*, 971–985. [CrossRef]
30. Chen, J.; Thapa, A.K.; Berfield, T.A. In-situ characterization of strain in lithium battery working electrodes. *J. Power Sources* **2014**, *271*, 406–413. [CrossRef]
31. Leung, P.K.; Moreno, C.; Masters, I.; Hazra, S.; Conde, B.; Mohamed, M.R.; Dashwood, R.J.; Bhagat, R. Real-time displacement and strain mappings of lithium-ion batteries using three-dimensional digital image correlation. *J. Power Sources* **2014**, *271*, 82–86. [CrossRef]
32. Scarminio, J.; Sahu, S.N.; Decker, F. In situ measurements of the stress changes in thin-film electrodes. *J. Phys. E Sci. Instrum.* **1989**, *22*, 755. [CrossRef]
33. Rosolen, J.M.; Decker, F. Stress in carbon film electrodes during Li+ electrochemical intercalation. *J. Electrochem. Soc.* **1996**, *143*, 2417. [CrossRef]
34. Pyun, S.I.; Go, J.Y.; Jang, T.S. An investigation of intercalation-induced stresses generated during lithium transport through $Li1-\delta CoO_2$ film electrode using a laser beam deflection method. *Electrochim. Acta* **2004**, *49*, 4477–4486. [CrossRef]

35. Tavassol, H.; Chan, M.K.; Catarello, M.G.; Greeley, J.; Cahill, D.G.; Gewirth, A.A. Surface coverage and SEI induced electrochemical surface stress changes during Li deposition in a model system for Li-ion battery anodes. *J. Electrochem. Soc.* **2013**, *160*, A888. [CrossRef]
36. Chung, K.Y.; Kim, K.B. Investigation of structural fatigue in spinel electrodes using in situ laser probe beam deflection technique. *J. Electrochem. Soc.* **2001**, *149*, A79. [CrossRef]
37. Chason, E.; Sheldon, B.W. Monitoring stress in thin films during processing. *Surf. Eng.* **2003**, *19*, 387–391. [CrossRef]
38. Mukhopadhyay, A.; Guo, F.; Tokranov, A.; Xiao, X.; Hurt, R.H.; Sheldon, B.W. Engineering of Graphene Layer Orientation to Attain High Rate Capability and Anisotropic Properties in Li-Ion Battery Electrodes. *Adv. Funct. Mater.* **2013**, *23*, 2397–2404. [CrossRef]
39. Mukhopadhyay, A.; Tokranov, A.; Sena, K.; Xiao, X.; Sheldon, B.W. Thin film graphite electrodes with low stress generation during Li-intercalation. *Carbon* **2011**, *49*, 2742–2749. [CrossRef]
40. Sethuraman, V.A.; Chon, M.J.; Shimshak, M.; Van Winkle, N.; Guduru, P.R. In situ measurement of biaxial modulus of Si anode for Li-ion batteries. *Electrochem. Commun.* **2010**, *12*, 1614–1617. [CrossRef]
41. Sethuraman, V.A.; Van Winkle, N.; Abraham, D.P.; Bower, A.F.; Guduru, P.R. Real-time stress measurements in lithium-ion battery negative-electrodes. *J. Power Sources* **2012**, *206*, 334–342. [CrossRef]
42. Nadimpalli, S.P.; Sethuraman, V.A.; Abraham, D.P.; Bower, A.F.; Guduru, P.R. Stress evolution in lithium-ion composite electrodes during electrochemical cycling and resulting internal pressures on the cell casing. *J. Electrochem. Soc.* **2015**, *162*, A2656. [CrossRef]
43. Klink, J.; Hebenbrock, A.; Grabow, J.; Orazov, N.; Nylén, U.; Benger, R.; Beck, H.P. Comparison of model-based and sensor-based detection of thermal runaway in Li-ion battery modules for automotive application. *Batteries* **2022**, *8*, 34. [CrossRef]
44. Lee, C.Y.; Peng, H.C.; Lee, S.J.; Hung, I.M.; Hsieh, C.T.; Chiou, C.S.; Chang, Y.M.; Huang, Y.P. A flexible three-in-one microsensor for real-time monitoring of internal temperature, voltage and current of lithium batteries. *Sensors* **2015**, *15*, 11485–11498. [CrossRef] [PubMed]
45. Lee, C.Y.; Lee, S.J.; Hung, Y.M.; Hsieh, C.T.; Chang, Y.M.; Huang, Y.T.; Lin, J.T. Integrated microsensor for real-time microscopic monitoring of local temperature, voltage and current inside lithium ion battery. *Sens. Actuators A Phys.* **2017**, *253*, 59–68. [CrossRef]
46. Ge, L.; Yao, B.; Guo, Y. A Lithium Battery Thermal Runaway Monitoring Alarm Sensing Device. CN111799248A, 23 June 2020.
47. Xie, Q.; Luo, Q.; Cheng, S. Overview of contact temperature measurement technology. *China Instrum. Meters* **2017**, 48–53.
48. Tu, Z.; Jiang, C.; Tu, Q.; Zhu, C.; Huang, H. Summary of Sensorless Control Technology for Permanent Magnet Synchronous Motors Used in Electric Vehicles. *Micromotors* **2022**, *11*, 56. [CrossRef]
49. Lin, C.; Xu, Y.; Xing, J.; Zhuang, X.; Jiang, X. Overview of Drive and Control Technology for Vehicle Ultra High Speed Permanent Magnet Motors. *Automot. Eng.* **2022**, *44*, 1049r1058. [CrossRef]
50. Stipetic, S.; Kovacic, M.; Hanic, Z.; Vrazic, M. Measurement of excitation winding temperature on synchronous generator in rotation using infrared thermography. *IEEE Trans. Ind. Electron.* **2011**, *59*, 2288–2298. [CrossRef]
51. Shen, B. Temperature Monitoring System for Steel Rolling Motors. *Metall. Autom.* **1982**, 22–26.
52. Zhu, H.; Wang, Y. Feasibility of using temperature controlled thyristors for motor temperature sensors. *Coal Mine Autom.* **1993**, 37–39+66.
53. Wang, R.; Ma, Y.; Ma, Q. Multi point temperature measurement and control system for hoists. In *Proceedings of the Paper Album of the 11th National Coal Mine Automation Academic Annual Conference, China Coal Society*; Editorial Department of Coal Mine Automation: Tongchuan, China, 2001; pp. 95–98.
54. Yang, R. Research on Motor Temperature Monitoring System Based on Piezoelectric Energy Acquisition and Power Supply. Master's Thesis, North China Electric Power Science, Beijing, China, 2021.
55. Zhang, Z. Technical research on rotor temperature measurement of large and medium-sized electric machines. *Shanghai Large Medium Electr. Mach.* **2002**, *32*, 37–40. [CrossRef]
56. Huang, Y.; Chen, Z. Research on rotor temperature measurement and excitation system fault diagnosis and treatment of brushless synchronous motors. *J. Electr. Technol.* **1992**, 2–5.
57. Feng, Y.; Chen, Q.; Shi, H. Online Detection Technology of Brushless Excitation Generator Rotor Current and Temperature. *J. Instrum. Appar.* **2001**, *22*, 1. [CrossRef]
58. Ren, P. Analysis of Rotor Temperature Measurement Method for Large Brushless Excitation Generator in Nuclear Power Plant. *Electr. Power Sci. Eng.* **2007**, *23*, 59–61. [CrossRef]
59. Ren, P. Review of rotor temperature measurement methods for large brushless excitation generators in nuclear power plants. *Electr. Power Constr.* **2007**, *28*, 55–56. [CrossRef]
60. Chen, W.; Chen, Z.; Zhu, Q.; Song, Z. A method and implementation of motor rotor temperature measurement. *Mod. Meas. Lab. Manag.* **2010**, *18*, 3–5. [CrossRef]
61. Feng, J.; Yuan, C.; Wei, Y.; Chen, Z. Online Monitoring of Motor Rotor Temperature Based on SMS Technology (I)—System Principle and Hardware Composition. *Electr. Power Autom. Equip.* **2008**, *28*, 103–106. [CrossRef]
62. Wu, Q.; Su, Z. Wireless temperature measurement based on HT48XXX series MCU. *Micro Spec. Electr. Mach.* **2007**, *35*, 61–62. [CrossRef]
63. Sui, M. Research on Real-Time Temperature Measurement Technology of Electric Motor. Master's Thesis, Shenyang University of Technology, Shenyang, China, 2008.

64. Zhao, X.; Cheng, X.; Long, Y. A New Method for Measuring the Temperature of Hydrogenerator Rotor. *Sci. Technol. Inf.* **2014**, 8–9. [CrossRef]
65. Wu, B.; Wang, K.; Lu, F.; Huang, S.; He, G.; Tong, X. Simulation test research on steam turbine rotor surface temperature measurement. *Chin. J. Power Eng.* **2011**, *31*, 421–426.
66. Liu, J. Rotor Temperature Measurement of Large Brushless Excitation Generator. *Value Eng.* **2010**, *29*, 17–18. [CrossRef]
67. Zhu, W. Research on Eddy Current Loss and Temperature Field of Rotor Permanent Magnet of Electric Vehicle Permanent Magnet Synchronous Motor. Master's Thesis, Beijing Institute of Technology, Beijing, China, 2014.
68. Wu, X. Research on High-Efficiency Calculation Method of Global Loss of Surface-Mounted Permanent Magnet Synchronous Motor for Vehicles. Ph.D. Thesis, Beijing Institute of Technology, Beijing, China, 2016.
69. Sun, Q. Research on Online Estimation of Stator Temperature of Permanent Magnet Synchronous Motor for Electric Vehicles. Master's Thesis, Hunan University, Changsha, China, 2018.
70. Li, B.; Sun, J.; Li, H. Three-dimensional thermal network model of axially ventilated permanent magnet synchronous motor. *J. Tianjin Univ. Nat. Sci. Eng. Technol. Ed.* **2016**, *49*, 1161–1166. [CrossRef]
71. Nategh, S.; Huang, Z.; Krings, A.; Wallmark, O.; Leksell, M. Thermal modeling of directly cooled electric machines using lumped parameter and limited CFD analysis. *IEEE Trans. Energy Convers.* **2013**, *28*, 979–990. [CrossRef]
72. Boglietti, A.; Cavagnino, A.; Staton, D.; Shanel, M.; Mueller, M.; Mejuto, C. Evolution and modern approaches for thermal analysis of electrical machines. *IEEE Trans. Ind. Electron.* **2009**, *56*, 871–882. [CrossRef]
73. Huber, T.; Peters, W.; Bocker, J. A low-order thermal model for monitoring critical temperatures in permanent magnet synchronous motors. In *IET Conference Proceedings*; The Institution of Engineering & Technology: London, UK, 2014.
74. Kral, C.; Haumer, A.; Lee, S.B. A practical thermal model for the estimation of permanent magnet and stator winding temperatures. *IEEE Trans. Power Electron.* **2013**, *29*, 455–464. [CrossRef]
75. Fan, J.; Zhang, C.; Wang, Z.; Dong, Y.; Nino, C.E.; Tariq, A.R.; Strangas, E.G. Thermal analysis of permanent magnet motor for the electric vehicle application considering driving duty cycle. *IEEE Trans. Magn.* **2010**, *46*, 2493–2496. [CrossRef]
76. Wallscheid, O.; Böcker, J. Design and identification of a lumped-parameter thermal network for permanent magnet synchronous motors based on heat transfer theory and particle swarm optimization. In Proceedings of the 2015 17th European Conference on Power Electronics and Applications (EPE'15 ECCE-Europe), Geneva, Switzerland, 8–10 September 2015; IEEE: New York, NY, USA, 2015; pp. 1–10.
77. Nategh, S.; Wallmark, O.; Leksell, M.; Zhao, S. Thermal analysis of a PMaSRM using partial FEA and lumped parameter modeling. *IEEE Trans. Energy Convers.* **2012**, *27*, 477–488. [CrossRef]
78. Kuehbacher, D.; Kelleter, A.; Gerling, D. An improved approach for transient thermal modeling using lumped parameter networks. In Proceedings of the 2013 International Electric Machines & Drives Conference, Chicago, IL, USA, 12–15 May 2013; IEEE: New York, NY, USA, 2013; pp. 824–831.
79. Wallscheid, O.; Böcker, J. Global identification of a low-order lumped-parameter thermal network for permanent magnet synchronous motors. *IEEE Trans. Energy Convers.* **2015**, *31*, 354–365. [CrossRef]
80. Demetriades, G.D.; De La Parra, H.Z.; Andersson, E.; Olsson, H. A real-time thermal model of a permanent-magnet synchronous motor. *IEEE Trans. Power Electron.* **2009**, *25*, 463–474. [CrossRef]
81. Jiang, S.; Wang, L.; Wang, L.; Ye, P.; Hao, Z. A new thermal protection approach for permanent magnet synchronous motor. In Proceedings of the IECON 2013-39th Annual Conference of the IEEE Industrial Electronics Society, Vienna, Austria, 10–13 November 2013; IEEE: New York, NY, USA, 2013; pp. 2536–2540.
82. Kylander, G. *Thermal Modelling of Small Cage Induction Motors*; Chalmers Tekniska Hogskola: Göteborg, Sweden, 1995.
83. Andersson, E. *Real Time Thermal Model for Servomotor Applications*; Technical Report; ABB Corporate Research: Stockholm, Sweden, 2006.
84. Boglietti, A.; Cavagnino, A.; Staton, D. Determination of critical parameters in electrical machine thermal models. *IEEE Trans. Ind. Appl.* **2008**, *44*, 1150–1159. [CrossRef]
85. Seong, K.H.; Hwang, J.; Shim, J.; Cho, H.W. Investigation of temperature rise in an induction motor considering the effect of loading. *IEEE Trans. Magn.* **2014**, *50*, 1–4. [CrossRef]
86. Hey, J.; Malloy, A.C.; Martinez-Botas, R.; Lampérth, M. Online monitoring of electromagnetic losses in an electric motor indirectly through temperature measurement. *IEEE Trans. Energy Convers.* **2016**, *31*, 1347–1355. [CrossRef]
87. Zhu, Y.; Xiao, M.; Lu, K. Rotor Temperature Estimation of Electric Vehicle Permanent Magnet Synchronous Motor. *Electr. Mach. Control.* **2021**, *25*, 72–81.
88. Zhang, H. Online thermal monitoring models for induction machines. *IEEE Trans. Energy Convers.* **2015**, *30*, 1279–1287. [CrossRef]
89. Paice, D.A. Motor thermal protection by continuous monitoring of winding resistance. *IEEE Trans. Ind. Electron. Control. Instrum.* **1980**, *IECI-27*, 137–141. [CrossRef]
90. Zhang, P.; Du, Y.; Lu, B.; Habetler, T.G. A DC signal injection-based thermal protection scheme for soft-starter-connected induction motors. *IEEE Trans. Ind. Appl.* **2009**, *45*, 1351–1358. [CrossRef]
91. Lee, S.B.; Habetler, T.G. An online stator winding resistance estimation technique for temperature monitoring of line-connected induction machines. *IEEE Trans. Ind. Appl.* **2003**, *39*, 685–694. [CrossRef]
92. Zhang, P.; Lu, B.; Habetler, T.G. An active stator temperature estimation technique for thermal protection of inverter-fed induction motors with considerations of impaired cooling detection. *IEEE Trans. Ind. Appl.* **2010**, *46*, 1873–1881. [CrossRef]

93. Cheng, S.; Du, Y.; Restrepo, J.A.; Zhang, P.; Habetler, T.G. A nonintrusive thermal monitoring method for induction motors fed by closed-loop inverter drives. *IEEE Trans. Power Electron.* **2012**, *27*, 4122–4131. [CrossRef]
94. Liu, P.; Sun, Q.; Ye, J.; Tu, C. Online Estimation of Stator Winding Temperature of Permanent Magnet Synchronous Motor Based on DC Voltage Injection. *J. Electrotech. Soc.* **2017**, *32*, 198–204.
95. Wilson, S.D.; Stewart, P.; Taylor, B.P. Methods of resistance estimation in permanent magnet synchronous motors for real-time thermal management. *IEEE Trans. Energy Convers.* **2010**, *25*, 698–707. [CrossRef]
96. Kellner, S.L.; Piepenbreier, B. Identification of ohmic stator resistance based on low frequency current signal injection in permanent magnet synchronous machines. In Proceedings of the 14th International Power Electronics and Motion Control Conference EPE-PEMC 2010, Ohrid, Macedonia, 6–8 September 2010; IEEE: New York, NY, USA, 2010; pp. T5-221–T5-229. [CrossRef]
97. Reigosa, D.; Fernández, D.; Diez, A.B.; Guerrero, J.M.; Briz, F. Thermal and magnetization state monitoring of PMSM drives using HF signal injection. In Proceedings of the 2017 IEEE Workshop on Electrical Machines Design, Control and Diagnosis (WEMDCD), Nottingham, UK, 20–21 April 2017; IEEE: New York, NY, USA, 2017; pp. 298–306.
98. Hang, J.; Zhang, Y.; Ding, S.; Huang, Y.; Wang, Q. A torque-injection-based method for stator temperature estimation of direct-torque-controlled permanent magnet synchronous motors. In Proceedings of the 2017 20th International Conference on Electrical Machines and Systems (ICEMS), Sydney, NSW, Australia, 11–14 August 2017; IEEE: New York, NY, USA, 2017; pp. 1–5.
99. Zhang, S.; Li, S.; He, L.; Restrepo, J.A.; Habetler, T.G. A high-frequency torque injection-based rotor thermal monitoring scheme for direct-torque-controlled interior permanent magnet synchronous machines. In Proceedings of the 2017 IEEE Energy Conversion Congress and Exposition (ECCE), Cincinnati, ON, USA, 1–5 October 2017; IEEE: New York, NY, USA, 2017; pp. 3552–3558.
100. He, L.; Cheng, S.; Du, Y.; Harley, R.G.; Habetler, T.G. A DC-flux-injection approach for thermal monitoring of induction machines with direct torque control. In Proceedings of the 2013 IEEE Energy Conversion Congress and Exposition, Denver, CO, USA, 15–19 September 2013; IEEE: New York, NY, USA, 2013; pp. 2115–2122.
101. Zhang, S.; Li, S.; He, L.; Restrepo, J.A.; Habetler, T.G. A high-frequency rotating flux injection based rotor thermal monitoring scheme for direct-torque-controlled interior permanent magnet synchronous machines. In Proceedings of the 2017 IEEE International Electric Machines and Drives Conference (IEMDC), Miami, FL, USA, 21–24 May 2017; IEEE: New York, NY, USA, 2017; pp. 1–6.
102. He, L.; Restrepo, J.; Cheng, S.; Harley, R.G.; Habetler, T.G. An improved DC-signal-injection method with active torque-ripple mitigation for thermal monitoring of field-oriented-controlled induction motors. In Proceedings of the 2015 IEEE Energy Conversion Congress and Exposition (ECCE), Montreal, QC, Canada, 20–24 September 2015; IEEE: New York, NY, USA, 2015; pp. 4447–4454.
103. Li, S.; Zhang, S.; Jiang, C.; He, L.; Harley, R.G. An enhanced active DC-flux injection based approach for thermal monitoring of induction machines with direct torque control schemes. In Proceedings of the 2017 IEEE Energy Conversion Congress and Exposition (ECCE), Cincinnati, ON, USA, 1–5 October 2017; IEEE: New York, NY, USA, 2017; pp. 3537–3544.
104. Wang, Y.; Niimura, N.; Lorenz, R.D. Real-time parameter identification and integration on deadbeat-direct torque and flux control (DB-DTFC) without inducing additional torque ripple. *IEEE Trans. Ind. Appl.* **2016**, *52*, 3104–3114. [CrossRef]
105. He, L.; Cheng, S.; Du, Y.; Harley, R.G.; Habetler, T.G. Stator temperature estimation of direct-torque-controlled induction machines via active flux or torque injection. *IEEE Trans. Power Electron.* **2014**, *30*, 888–899. [CrossRef]
106. Huang, X.; Tan, Q.; Li, L.; Li, J.; Qian, Z. Winding temperature field model considering void ratio and temperature rise of a permanent-magnet synchronous motor with high current density. *IEEE Trans. Ind. Electron.* **2016**, *64*, 2168–2177. [CrossRef]
107. Wallscheid, O.; Böcker, J. Fusion of direct and indirect temperature estimation techniques for permanent magnet synchronous motors. In Proceedings of the 2017 IEEE International Electric Machines and Drives Conference (IEMDC), Miami, FL, USA, 21–24 May 2017; IEEE: New York, NY, USA, 2017; pp. 1–8.
108. Lv, X. Research on Numerical Simulation and Temperature Identification Technology of Temperature Field of Submersible Motor. Ph.D. Thesis, Harbin Institute of Technology, Harbin, China, 2013.
109. Zhang, P.; Du, Y.; Habetler, T.G.; Lu, B. Magnetic effects of DC signal injection on induction motors for thermal evaluation of stator windings. *IEEE Trans. Ind. Electron.* **2010**, *58*, 1479–1489. [CrossRef]
110. Sun, J. Motor Winding Temperature Identification and Reconstruction Based on Signal Injection and Thermal Network Method. Master's Thesis, Shenyang Industrial Science, Shenyang, China, 2022. [CrossRef]
111. Chen, M. Automotive Air Conditioning. *Refrig. Technol.* **1995**, 16–22.
112. Zhang, L. Classification and Development Trend of Automotive Sensors. *Ind. Instrum. Autom. Devices* **2015**, 16–18. [CrossRef]
113. Jin, M.; Zhang, Q. Application and Types of Automotive Air Conditioning Sensors. *Automob. Electr. Appl.* **2017**, 71–73. [CrossRef]
114. Bao, J. Research on Frosting in Air Conditioning System of Commercial Vehicles. *Automob. Electr. Appl.* **2019**, 67–69. [CrossRef]
115. Yang, Y. Research on temperature sensor location and control parameters optimization of automotive air conditioner. *Intern. Combust. Engines Accessories* **2018**, 196–197. [CrossRef]
116. Cai, C.; Guo, W. Improvement Research on Frequent Start-up of Automobile Air Conditioning in Idling State. *Refrig. Technol.* **2013**, *33*, 30–32. [CrossRef]
117. Dong, J.; Zhang, G.; Tang, Q.; Li, Y.; Huang, N. Experimental study on the characteristics of electric vehicle heat pump air conditioner condensing evaporator. *J. Refrig.* **2019**, *40*, 118–124.

118. Huang, W.; Ding, L.; Wang, B.; Shi, W. Research on field performance test method of air source heat pump based on compressor heat balance. In Proceedings of the Thirteenth National Refrigerator (Cabinet), Air Conditioner and Compressor Academic Exchange Conference 2016, Foshan, China, 9 December 2016.
119. Wu, L.; Ai, M. Overheating damage analysis and countermeasures of variable frequency rotary compressor. *Refrig. Air Cond.* **2021**, *21*, 28–31. [CrossRef]
120. He, J.; Tao, L.; Yu, Z. Influence of Incomplete Superheating on Low-frequency Operation Performance of R32 Rotary Compressor. *Fluid Mach.* **2019**, *47*, 1–7.
121. Lu, G.; Sun, W. Influence of Compressor Exhaust Overheating on Air Conditioner Reliability. *Home Appl. Sci. Technol.* **2011**, 86–87. [CrossRef]
122. Cao, J.; Xu, G.; Dai, Y.; Li, T.; Niu, X. Compressor Condition Monitoring Based on Optical Fiber Sensor. *Opt. Optoelectron. Technol.* **2013**, *11*, 29–32.
123. Huang, B. Energy-saving control system based on multi-sensor information fusion. *Meas. Control. Technol.* **2013**, *32*, 66–69. [CrossRef]
124. Liu, Q. Research on Multi-Sensor Control Strategy of VAV Air Conditioning System Based on TRNSYS-FLUENT Co-Simulation. Master's Thesis, Shanghai Jiaotong University, Shanghai, China, 2013.
125. Ge, X. Control and Optimization of Variable Air Volume Air Conditioning System Based on TRNSYS-FLUENT Co-Simulation. Master's Thesis, Shanghai Jiao Tong University, Shanghai, China, 2017.
126. Fang, H.; Li, J.; He, J.; Wu, Y. Research Progress on Sensor Fault Diagnosis of Air Conditioning System. *Clean Air Cond. Technol.* **2017**, 90–94. [CrossRef]
127. Usoro, P.B.; Schick, I.C.; Negahdaripour, S. An innovation-based methodology for HVAC system fault detection. *J. Dyn. Syst. Meas. Control* **1985**, *107*, 284–289. [CrossRef]
128. Wang, S.; Chen, Y. Fault-tolerant control for outdoor ventilation air flow rate in buildings based on neural network. *Build. Environ.* **2002**, *37*, 691–704. [CrossRef]
129. Lee, W.Y.; House, J.M.; Shin, D.R. *Fault Diagnosis and Temperature Sensor Recovery for an Air-Handling Unit*; American Society of Heating, Refrigerating & Air-Conditioning Engineers: Atlanta, GA, USA, 1997.